Radiant glass façade technology: Thermal and comfort performance based on experimental monitoring of outdoor test cells.

Corresponding author:

Giuseppe La Ferla.

Departamento de Construcción y Tecnología Arquitectónicas, Escuela Técnica Superior de Arquitectura de Madrid. Universidad Politécnica de Madrid.

Av. Juan de Herrera, 4. 28040. Madrid. Spain.

g.laferla.licitra@gmail.com

0034 678621327

Authors:

Consolación Ana Acha Román.

Departamento de Construcción y Tecnología Arquitectónicas, Escuela Técnica Superior de Arquitectura de Madrid. Universidad Politécnica de Madrid.

Av. Juan de Herrera, 4, 28040, Madrid, Spain

consolacionana.acha@upm.es

Jaime Roset Calzada.

Departamento Física, Escuela Técnica Superior de Arquitectura de Barcelona, Universitat Politècnica de Catalunya.

Avda. Diagonal, 649. 08028 Barcelona. Spain

jaime.roset@upc.edu

Highlights

- Radiant asymmetry in a glazed façade is addressed using radiant glass technology
- Thermal comfort performance of radiant glass is compared with that of conventional glass
- Radiant glass improves thermal comfort levels near the perimeter zone of a glazed façade
- Operative temperature can be maintained by reducing MRT, air, or surface temperatures
- Isotherm distribution of radiant temperature from radiant glass was studied

Abstract

Fully glazed façades on commercial buildings have a significant impact on the thermal comfort of the occupants. Discomfort caused by thermal asymmetry can be addressed with a commercial glass curtain wall equipped with radiant glass (RG) technology. Such a wall acts as a heating system that uses radiant long-wave heat, and is fully integrated into the façade; the thermal performance of a glass curtain wall can be adapted according to occupant requirements.

This study presents the results of an experimental campaign of tests conducted in outdoor test cells equipped with RG to assess the thermal and comfort performance of the façade.

The study compares two identical cells in the same boundary under winter climate conditions: one (as reference) with a commercial low-e double glass façade and an HVAC heating system, and the other (as prototype) equipped with RG technology working entirely as the heating system. Comparisons between data gathered from outdoor cells were performed to investigate the thermodynamic performance, radiant and thermal asymmetry, operative and air temperatures, standards, and local indoor thermal comfort levels of both façades.

This study demonstrated that using RG as a heating device can improve the level of thermal comfort by avoiding radiant asymmetry through a uniform distribution of radiant temperature, even along the perimeter zone in higher-glazed façades not subjected to external climatic conditions. The results suggests that operative and ambient temperatures can be lowered while maintaining thermal comfort.

Keywords:

Radiant glass façade; electrically heated glass; thermal comfort; radiant thermal asymmetry; commercial building façade.

Nomenclature		
w	width	m
H	height	m
L	length	m
THt, T_roof	Interior roof surface temperature	°C
THo, T_wall_w	Interior west wall surface temperature	°C
THs, T_wall_s	Interior south wall surface temperature	°C
T_wall	Average interior envelope surface temperature	°C
THa, T_air	Interior air temperature in the center of the cell	°C
THi, T_glass_in	Mean glass surface temperature (interior pane)	°C
THx, T_glass_out	Mean glass surface temperature (exterior pane)	°C
T_cglass	Center glass surface temperature	°C
T_edglass	Everage edge glass surface temperature	°C
Tex, T_out	Exterior temperature	°C
HR	Relative humidity	%
Th	Thickness	m
t_o, t_op	Operative temperature in the center of the cell	°C
P	Atmospheric pressure	Pa
U*g*	Glass transmittance	W/m^2K
Wv	Wind velocity	Km/h

$\bar{t}_r$, t̄_r	Mean radiant temperature	°C
t_{pr}, t_pr	Plane radiant temperature	°C
Δt_{pr}	Radiant asymmetry	°C
v_{ar}	Relative air velocity	m/s
$F_{i,J}$	View factor between *n*-th space position and envelope	non-dim.
M	Metabolic rate	met
W	Activity level	met
I_{cl}	Thermal insulation of the clothing	clo
E	Solar irradiance	W/m^2
Tsol	Solar transmittance of the glazing	non-dim.
Rsol	Solar reflectance of the glazing	non-dim.
Absol	Solar absorbance of the glazing	non-dim.
Tvis	Visible transmittance of the glazing	non-dim.
Rvis	Visible reflectance of the glazing	non-dim.
Tuv	UV transmission of the glazing	non-dim.
K.eff	Effective thermal conductivity of the glazing	W/m·K
Layer 1, 2	Thermal conductivity of the glass layer 1 or 2	W/m·K
Gap	Thermal conductivity of the gas cavity	W/m·K
SC	Shading coefficient	non-dim.
SHGC	Solar heat gain coefficient	non-dim.
Subscripts		
i	*i*-th counter (i=1…9)	
j	*j*-th counter (j=1…9)	

n	*n*-th counter (n=1….81)
in	Interior
ex, out	Exterior, outdoor
max	Maximum
day	total daily value

1

1. Introduction

In contemporary architecture, fully glazed buildings present a distinctive identity; most are commercial buildings for office use. The interior thermal comfort levels associated with these envelopes are a primary concern for the construction sector (industry and academic). Advanced fenestration systems attempt to address global environmental issues by changing performance through single-glazed glass (tinted, reflective, low-emissivity, smart, photovoltaic), double-glazed glass (gas filled, liquid filled or flow, evacuated), switchable glass (electrochromic, PMC) [1][2][3] and the newer concept of adaptive façades [4].

Human thermal sensation is mainly related to the thermal balance of the body, which is influenced by energy exchange with the environment, physical activity (metabolic heat production), clothing, and environmental parameters [5]. Thermal comfort can be influenced by asymmetric radiation fields near the glazed façade. Total or local discomfort (on a part of the body) can result from radiative heat exchange between a person and his surroundings, even if the overall heat balance is neutral [6]. One of the most common thermal discomfort factors is radiant temperature asymmetry (Δt_{pr}) caused by a warm or cold wall, ceiling or pavement.

Fanger et al. studied the impact of thermal radiation in ceilings [7], walls [8], and the limits of asymmetry. McIntyre et al. [9] and Griffiths et al. [10] studied the effect of the radiant heating ceiling systems on the thermal comfort. McNall et al. [11] investigated ceiling and wall surface temperatures to find a recommended vector of radiant temperature. However, Huizenga et al. [6] defined those studies as inconsistent, mainly because the results were significantly higher (10 ºC) than the results of Fanger (4 ºC) for a heated ceiling.

Fanger et al. [8] also defined the maximum value of radiant temperature asymmetry for warm (23 ºC) and cool (10 ºC) walls, and for warm (4 ºC) and cool (14 ºC) ceilings, defining the limits with 5% dissatisfaction caused by radiant asymmetry. The study found that people are more sensitive to a cool wall than a warm wall, that local cooling of the body caused more frequent discomfort than local heating, and that people are more sensitive to radiation asymmetry from heat on the feet. No significant differences in the impact on operative temperature were found. The results were included in the international standards ASHRAE 55 [12] and ISO 7730 [13]. Olesen et al. [14][15] studied the effect of floor temperature on comfort to find the optimal temperature.

The impact of the mean radiant temperature on thermal comfort in indoor environments is widely studied [16][17][18][19]. Zhang et al. [16] and Huizenga et al. [22] developed an advanced comfort model to predict sensations and comfort in transient and asymmetrical environments, They concluded that current limits specified in ASHRAE Standard-55 are too restrictive [20].

The thermal sensation for the entire body can be estimated in terms of the predicted mean vote (PMV) and predicted percentage of dissatisfied (PPD) categories, according to Fanger's definition and as described in ISO 7730 [13]. However, the model was based on uniform and stationary conditions, controlled in a climatic chamber [16]. The percentage dissatisfied (PD) can be determined as a function of the horizontal radiant asymmetry (from side-to-side) with respect to the body position relative to the considered front/back surfaces [16]. Local thermal discomfort can be defined as the sensation caused by unwanted local cooling or heating of a particular area of the body [23].

Recent studies underlined the relationships between mean radiant temperature, operative temperature and air temperature [24]. To archive thermal comfort it was recommended to use operative temperature sensor rather an air temperature device [25][26][27][28], although more recent works have shown mixed results [29]. Other researches specified that for radiant equipment it may not be necessary because they are almost satisfactory as all-air building systems [30][31]. Some simulations studies have investigated the effect of different types of glazing and windows dimensions [32] and experimental works have tested the risk of the draft effect in low-performance window [33].

International [24] and Spanish local regulations [35] recommend moderation of the effect of radiant asymmetry and prevention of global and local discomfort near highly-glazed perimeter zones, aiming to mitigate discomfort resulting from variability of the space using average values from the microclimatic parameters of the environment [23]. This is in contrast to the changing interior thermal surface conditions, which assume local differences in temperature in the same room space [36].

Contrary to convective heating, radiant technologies transfer energy partly by radiation and partly by convection [37], and they can be an alternative to air-based emitters. The large surface of exchange of radiant equipment allows the use of a source temperature close to the room temperature, thus increasing the efficiency of the system [37].

Radiant glass (RG), also known as electrically heated glass (EHG), is not a novel technology [38]; it has been used for heating in aircraft, refrigerator doors, cars, and recently to melt snow in a skylight atrium with a minimal slope.

Although RG is used in the building industry (IQ Glass Solutions LTD, SGG EGLAS, Radiant Glass Industries LLC, etc. are the main products), few studies have investigated its performance. Moreau et al. [39] demonstrated that RG reduces energy needs compared to a standard window with north, east, or west exposure. Kurnitski et al. [40] investigated the efficiency of RG and found it to be approximately 80% (depending on the exterior temperature), and also defined the equation to calculate it. Only a few experimental studies regarding RG energy efficiency performance have been conducted [41]. An investigation based on a simulation model was conducted to verify the effects on thermal comfort, but no experimental studies have been found with hanging outdoor conditions [42].

Hence, this research aims to contribute to the understanding of RG technology and its performance, focusing on thermal comfort performance.

In this study, a comparative methodology involving experimental data was used to evaluate the results.

The local distribution of thermal radiant asymmetry and indoor thermal comfort levels in the perimeter zone near the glazed façade were investigated.

The objectives were: i) to compare the performance of RG technology and standard glass during winter conditions; ii) to study the isotherm distribution of radiant temperature; iii) to analyse the thermal performance of the façade in terms of interior comfort indices; iv) to gather outdoor data for further modelling purposes.

2. Methodology

Two different research strategies can be used to investigate RG technology: i) mathematical model calculation and simulation; ii) experimental data obtained from physical models applied to mock-ups. Cattarin et al. [43] suggested the second method as the more appropriate and reliable methodology for this type of research. Experimental data permits comparison of technologies assembled in identical cells and climatic conditions using the same tools. The data and the results are directly comparable because they have the same errors and physics behaviours. Serra et al. [44] stated that there are several problems that depend on changing boundary conditions and management of the monitoring system, but the length of the monitoring period permits generalization of the data to statistic values.

The first step was definition of the radiant glass (RG) technology, the type of glass used, how it can be used as a radiant heating device, and how it operates (Section 3).

The characteristics of two identical cells used for the tests (the opaque envelope and the positions of the sensors) and the north exposure were defined. The M5 reference cell was used with a typical glass façade configuration, and the M6 prototype cell was equipped with RG. Single-pane features were gathered from the IGBD glass library in the WINDOW software [45] (Table 1 and Table 2); optical and centre glass features in glazed façade systems were calculated from WINDOW and OPTICS software [45] (Table 3 and Table 4).

The physics parameters were measured on the surface and at the centre of each cell (glazed and opaque envelopes); the control scheme of the RG and

HVAC temperatures and the air temperature of each cell were defined (Section 4.2).

Local weather conditions were characterized (Section 4.3) for comparison with the monitored period; a measurement campaign of 11 weeks was defined (from 16th December 2016 to 3rd March 2017).

Indoor operational temperatures were defined, including surface temperature of the RG and HVAC systems (as heating devices in each cell), and air temperatures in the centre of the cells (Section **Error! Reference source not found.**).

Data from the sensors and control systems were loaded, classified, and processed to derive features and calculations.

The main coefficients and parameters were calculated according to the referenced literature (Section 4.4):

- Glass transmittance (U*g*) was calculated with WINDOW software [45]
- Mean radiant temperature ($\bar{t}_r$), defined as the uniform temperature of an imaginary enclosure in which radiant heat transfer from the human body is equal to the radiant heat transfer in an actual non-uniform enclosure [46], was calculated (according to ISO 7726 [47]) from the temperature of the interior surrounding surfaces (T_i) and an angle factor (F_{P-A_i}) between a subject and the surroundings: $\overline{T^4}_r = \sum_{i=1}^{N} T_i^4 \cdot F_{P-A_i}$
- The view factor, defined as the angle factor between a subject (P) and the internal surrounding surfaces (A_i), as a function of the shape, size, and relative positions of the surfaces in relation to the subject, was calculated according to the algorithm defined by Cannistraro et al. [48]: $F_{P-A_i} =$

$F_{max}\left[1-e^{-(X1)/\tau}\right]\left[1-e^{-(Y1)/\gamma}\right]$ where $\tau = A + B\frac{a}{c}$ and $\gamma = C + D\frac{b}{c} + E\frac{a}{c}$ depends on the parameters (*A, B, C, D, E* and F_{max}) of the surface positions relative to the subject's orientation and posture, and *a, b, c* are the width, height and distance of the interior surfaces to the subject.

- Plane radiant temperature (t_{pr}), defined as the uniform temperature of an enclosure where the radiative flux on one side of a small plane element is the same as in the non-uniform actual environment [8], was calculated according to the ISO 7726 [47]: $T_{pr}^4 = T_1^4 F_{P-1} + T_2^4 F_{P-2} + \cdots + T_N^4 F_{P-N}$ where $F_{d1-2} = \frac{1}{2\pi}\left(tan^{-1}\frac{1}{Y_2} - \frac{Y_2}{\sqrt{{X_2}^2+{Y_2}^2}}tan^{-1}\frac{1}{\sqrt{{X_2}^2+{Y_2}^2}}\right)$ is the formula for calculating view factors for small plane element perpendicular to the rectangular surface, $F_{d1-2} = \frac{1}{2\pi}\left(\frac{X_3}{\sqrt{1+{X_3}^2}}tan^{-1}\frac{Y_3}{\sqrt{1+{X_3}^2}} + \frac{X_3}{\sqrt{1+{Y_3}^2}}tan^{-1}\frac{X_3}{\sqrt{1+{Y_3}^2}}\right)$ for small plane parallel, and where $X_2 = \frac{a}{b}$ $Y_2 = \frac{c}{b}$ $X_3 = \frac{a}{c}$, $Y_3 = \frac{b}{c}$ are the geometry parameters.
- Radiant temperature asymmetry (Δt_{pr}), defined as the difference between the plane radiant temperatures of the two opposite sides of a small element was calculated according to the ISO 7726 [47]: $\Delta t_{pr} = \left|T_{pr1} - T_{pr2}\right|$
- Operative temperatures (t_o), defined as the uniform temperature of an enclosure in which an occupant exchanges the same amount of heat by radiation plus convection as in the existing non-uniform environment, was calculated from the air temperature and mean radiant temperature in the

centre of the cells according to the ISO 7726 [47]:

$$t_o = {t_a\sqrt{10v_a} + \bar{t}_r}\Big/{1 + \sqrt{10v_a}}$$

- Indices PMV, PPD, and PD were calculated according to the ISO 7730 [13], and the assumptions for the calculation (metabolic rate, effective mechanical power, thermal insulation of clothing, and air velocity) were based on winter conditions.

The 'statistic day' was defined as the day configured from the average of the weather parameters data from each hour for the entire monitoring period. A 'typical day' was also considered in the monitoring period, comparable to the 'statistic day', with similar weather (Figure 3).

Three characteristic cases were selected from the monitoring period: the warmest and coldest days as two extreme conditions, and one typical day.

'Local performance' was defined as the sets of values assumed at several points uniformly distributed along a horizontal plane (at 0.6 m from the floor, considering a seated occupant), equivalent to the horizontal radiant plane defined by Cannistraro et al. [48] for the $\bar{t}_r$ calculations.

For comparative analysis and graphical superposition of the data and calculation results (for the two cells and the three cases in the study), two types of figures are presented:

- Daily comparison of the envelope surface temperatures (Figure 4 and Figure 5), daily comparison of operative, air temperatures (Figure 6 and Figure 7) and mean radiant and air temperatures in the centre of the cells (Figure 8), comparison as line representation of the daily distribution of the PMV indices (calculate in the centre of the cells and according to ISO 7730), and

comparison as bar representation of the frequency distribution of the indices (according to ISO 15251 [49]) in three main characteristics periods (according to curve behaviours) during the day (Figure 13).

- Comparison in the perimeter zone (by means of the local distribution at each point of the grid) of the mean radiant temperature $\bar{t}_r$ (Figure 9 and Figure 10), the radiant asymmetry temperature Δt_{pr} (Figure 11 and Figure 12), and local distribution of thermal environment indices (Figure 14 and Figure 15).

Thermal comfort performances were compared via daily performance and local distribution in the cells.

From the discussion of the results and analysis, conclusions were drawn to verify the objectives of the study.

3. Description of the technology

Radiant glass technology (RG) consists of a commercial low-emissivity glass with electrical power applied. The principle is based on the electrically insulating property of the glass (as support) and the semiconductor property of the layer coated on one side. Transparent conductive oxides (TCOs) are thin layers deposited on the glass, constructed from a combination of a primary metal and a secondary oxide semiconductor material [50]. The most common TCO in the industry is indium tin oxide (ITO), owing to its electrical and optical properties. TCOs are applied to low-emissivity glass in high-performance glazing to obtain good optical transmission at visible wavelengths and reflective properties at near-infrared wavelengths.

Due to its metal composition, electric power inducted with cathode and anode bus-bars along two opposite edges of the glass allow operation as a

semiconductor that produces heat radiation from electrical resistance according to Joule's law [51].

The RG used in this research is composed of a laminated low-e double pane glass filled with gas that is electrified and radiates towards the opposite face. The surface temperature of the RG glass panel and the air temperature were regulated by sensors connected with thermostats and the power regulator.

To reduce heat losses to the outside environment, the exterior pane is also coated on face #2 with a low-e layer. As a result, the glass acts as an infrared reflector to the radiation emitted by the interior glass [52] (Figure 1). The configurations of each glazed system are described in Section 4.1.

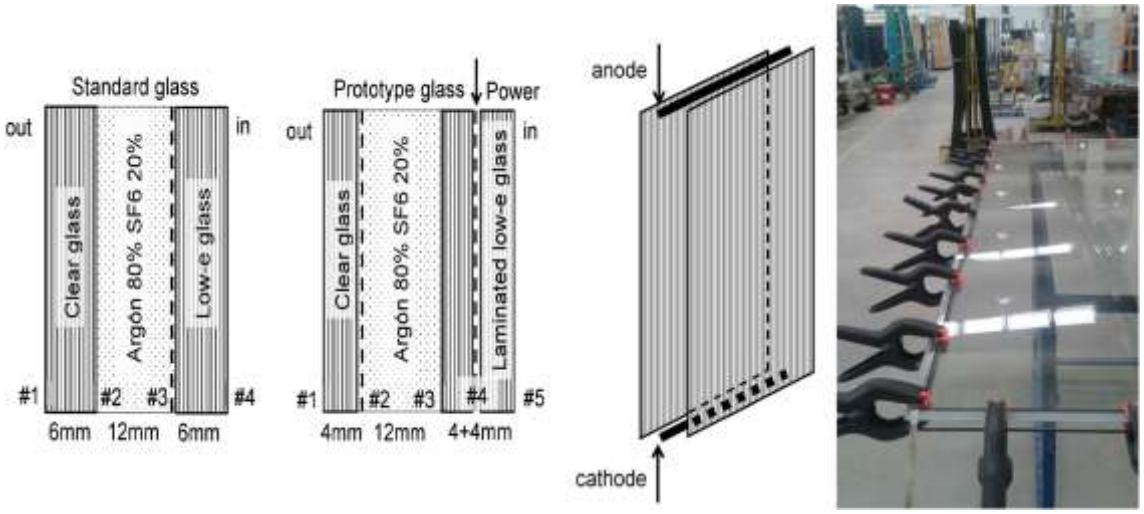

Figure 1. Technology diagrams and factory assembly process

4. Experiment set up

In this study, two identical modules were used: an M5 cell equipped with a standard glazed façade (as reference) and an M6 cell equipped with radiant glass technology (as experimental prototype).

The two monitored outdoor cells were located in the GESLAB outdoor facility (Figure 2) of the Polytechnic University of Madrid [53].

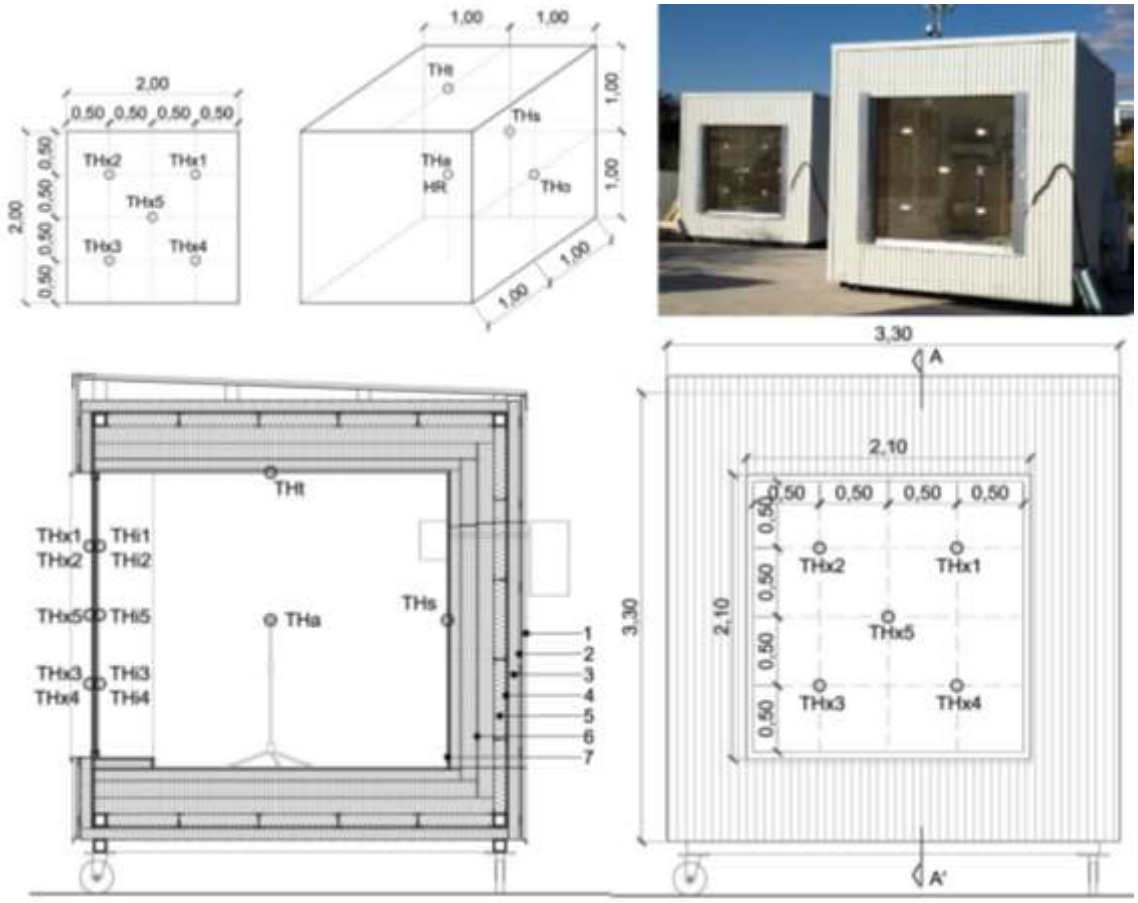

Figure 2. Cell configuration and sensor positions in the glass (THx, THi), inside the cell (THt, THs, THo, THa, HR), section, front elevation and exterior view of the cells in the GESLAB facility

The equal boundary conditions and construction typology of the cells produce comparable data allowing accurate comparisons between the two façades. The cells have exterior dimensions of 3.3 m wide, 3.3 m long, and 3.3 m high, with 2.1 m x 2.1 m x 2.1 m interior dimensions.

To avoid the influence of direct solar beam radiation and to maximize the necessity for a heating system, the cells were positioned for northward exposure.

The envelope of the cell (walls, floor, and roof) has 522 mm of total thickness and is composed of (from outside to inside):

1. Grey metallic panel as a rain screen (not considered in the total thickness).
2. Ethylene propylene diene monomer (EPDM) as a waterproofing membrane.
3. 80 mm of extruded polystyrene (XPS) thermal insulation panel.
4. 16 mm of oriented strand board (OSB) composite wood panel.
5. 70 mm of glass wool with a vapour barrier between the steel frame structures (tube 90x90x5 mm).
6. 120 mm +120 mm + 80 mm XPS panel (th = 320 mm total).
7. 16 mm OSB panel.

With a final U-value of 0.077 W/m²K, the envelope could be considered as an adiabatic envelope compared to the glazed envelope.

Both cells were equipped with an HVAC split unit system with a 2650-W cooling and a 3050-W heating capacity, 460 m³/h flow rate, and 1.0 °C of tolerance for temperature setting. In the reference cell (M5), the unit was used for heating; in the prototype cell (M6), only the RG was used for heating. No controller or device was used to regulate the relative humidity or air renewal parameters.

The glass used (Table 1, Table 2):

- K-Glass tempered on-line coated glass by Pilkington
- Clear float tempered monolithic glass by Guardian.

The voltage and current used to maintain the RG at 31 ºC were 40 V and 1.5 A, respectively, yielding a power of 120 W/m^2.

Glass type	Visible			Solar			Emissivity	
	Tvis (front/ back) -	Rvis (front) -	Rvis (back) -	Tsol (front/ back) -	Rsol (front) -	Rsol (back) -	ε (front) -	ε (back) -
K-Glass 4	0.825	0.117	0.111	0.704	0.118	0.106	0.17	0.84
K-Glass 6	0.813	0.116	0.109	0.667	0.116	0.099	0.17	0.84
Clear glass 4	0.900	0.084	0.084	0.844	0.078	0.078	0.84	0.84
Clear glass 6	0.894	0.083	0.083	0.813	0.076	0.075	0.84	0.84

Table 1. Optical data of glass panes from the IGBD glass library of WINDOW [45]

Glass type	Thickness	Coefficients		Conductivity		Ug	Sheet Resistance
	mm	SC -	SHGC -	K.eff W/m·K	Layer W/m·K	$W/m^{2}\cdot K$	Rs Ω/sq
K-Glass 4	3.850	0.880	0.766	N/A	1.000	3.7	**13**
K-Glass 8	5.900	0.854	0.743	N/A	1.000	3.6	**13**
Clear glass 4	3.840	1.004	0.874	N/A	1.000	5.803	**N/A**
Clear glass 6	5.610	0.985	0.857	N/A	1.000	5.744	**N/A**

Table 2. Centre glass results calculated with WINDOW [45]

4.1 Glass configuration

The RG technology was operational when electrical power was applied to the low-e layer and connected with power to the controller circuit of the cell. A standard commercial glass for glazed façade was used.

The first phase of experiments used a glass configuration similar to the one studied by Moreau et al. [39] to produce comparable data. After an unexpected breakage (probably an intrinsic weakness related to the assembly) a laminated glass was used for the new RG system, introducing base-bars (contained between the two glass panels) during the lamination process and thereby eliminating imprecisions during production; moreover laminated glass is standard in curtain walls (inner pane) for security reasons, especially in public building façades.

The glazed system configuration for each cell (Table 3, Table 4, Figure 1):

- Reference unit (M5): clear float 6 mm, 12 mm mixture gas, low-e K-Glass 6 mm tempered
- Prototype RG unit (M6): low-e K-Glass 4 mm tempered, 12 mm mixture gas, low-e K-Glass 4 mm tempered + clear float 4 mm tempered

The gas was a mixture of 80% argon and 20% SF6 (sulphur hexafluoride).

Glass type	**Thickness**	**Visible**			**Solar**					**UV**
	mm	**Tvis -**	**Rvis (ex) -**	**Rvis (i) -**	**Tsol -**	**Rsol (ex) -**	**Rsol (in) -**	**Absol (ex) -**	**Absol (in) -**	**Tuv -**
M5	23.51	0.730	0.175	0.163	0.554	0.154	0.135	0.122	0.167	0.392
M6	23.55	0.629	0.225	0.243	0.454	0.181	0.205	0.207	0.036	0.301

Table 3. Optical data of the reference and RG glass systems calculated with WINDOW and OPTICS [45]

Glass type	Coefficients		Conductivity				Ug
Centre Glass	SC -	SHGC -	K.eff W/m·K	Layer 1 W/m·K	Gap W/m·K	Layer 2 W/m·K	$W/m^{2}\cdot K$
M5	0.802	0.697	0.066	1.000	0.035	1.000	1.860
M6	0.683	0.594	0.059	1.000	0.031	1.003	1.732

Table 4. Centre glass results of the reference and RG glass systems calculated with WINDOW and OPTICS [45]

4.2 Monitoring and control system

The monitoring system consists of a different typology of sensors and instruments available in the GESLAB [53] (Table 5):

- 3 thermocouples (THt, T_roof; THo T_wall_w; THs, T_wall_s) for the interior surface temperatures of the envelope
- 10 thermocouples for the interior (THi, T_glass_in) and exterior (THx, T_glass_out) surface temperatures of the glass
- 1 indoor thermo-hygrometer-CO2 sensor in the centre of the cell (THa, T_air)
- 2 NTC sensors (only in M6 cell) for air (THa, T_air) and inner surface temperature (THi5, T_cglass_in) of the glass
- 1 AC Enda Erpa1 (440-F-RS) power regulator to control the radiant power (only in M6)

Each cell has an exterior control cabinet for the data acquisition system, and to manage the sensors, with two energy meters for power consumption (Domotax Orbis).

The weather conditions were determined from a station (Vantage Pro 2 Plus) located in the facility area that measured the parameters illustrated in Figure 3.

Code	Measured parameter	Measurement range	Accuracy
TJ thermocouple	Surface temperature	-210 ºC ~ +760 ºC	±0.5 ºC
NTC (10K/343)	Surface and air temperature	-55 ºC ~ +125 ºC	±0.5 ºC
SCR110 Schneider	Air temperature	10 ºC - 35 ºC	±0.5 ºC
SCR110 Schneider	Relative Humidity	0-95% RH	±2% RH
WH7016E Shenzhen thermostat	Temperature	-9.9 ºC ~ 99.9 ºC	±1 ºC
ASG0908I IN Saivod	HVAC internal thermostat	-15 ºC ~ 48 ºC	±1 ºC

Table 5. Technical characteristics of the sensors from the manufacturer

Measurements were taken according to ISO 7726 [47]; all instruments meet the accuracy recommended in Table 2 of the ISO.

Assembly and calibration of the instrumentation were performed by a team from the ROBOLABO (Robotic and Control System Group of ETSIT, UPM).

To protect the thermocouple from direct solar radiation, thin aluminium foil was fixed over the sensor, according to the recommendations of Kalyanova et al. [54] and ISO 7726 [47].

Monitoring was performed at a scan rate of 1 minute, while an average scan rate of 10 minutes was used for the analysis. The positions of the sensors were

defined as shown in Figure 2**Error! Reference source not found.**. The glass and air temperatures were regulated with sensors positioned on the inner face of the glass (THi5, T_cglass_in position) and at the centre of the cell (T_air position).

4.3 Local climatic conditions

The GESLAB outdoor facilities are located at 40°24'16.5'' N, 3°50'00.7'' W (south-west of Madrid), where local weather conditions are classified between hot-dry summer Mediterranean climate (Csa) and cold semi-arid climate (BSk) [55], according to the Köppen-Geiger climate categories [56].

According to the National Meteorology Agency [57], from November to February the statistic daily mean temperature is 7.5 ºC (with maximum of 12.0 ºC and minimum of 3.1 ºC), and the relative humidity is 73%.

During the monitoring (same period), the measured daily mean temperature was 8.0 ºC (with maximum of 14.3 ºC and minimum of 3.1 ºC), and the relative humidity was 70.4%.

4.4 Performance parameters and assumptions

The room air temperature (T_air) measured in the centre of the cells was considered as the air temperature [58], and in both cells was fixed as 21 ºC. The interior RG surface temperature (T_glass_in) in M6 was fixed 30 ºC. The RG was operating 24 hours per day.

The research was conducted using the following parameters:

- The thermal transmittance U_g, mean radiant temperature ($\bar{t}_r$), plane radiant temperature (t_{pr}), operative temperature (t_o at the centre of the cells), and

radiant thermal asymmetry (Δt_{pr}) were calculated as defined in methodology section 2.

- The view factor $F_{i,J}$, comfort indices PMV, PPD, and PD were and evaluated as defined in section 2.
- Metabolic rate *M* = 1.2 (*met*) for sedentary activity.
- Effective mechanical power *W* = 0 (*met*).
- Thermal insulation of clothing for winter $\mathrm{I_{cl}}$ = 1 (*clo)*.
- Relative air velocity inside the cells v_{ar} = 0.1 (m/s).

We considered as a case study the typical day (case A), as defined in the methodology (Section 2) (Figure 3).

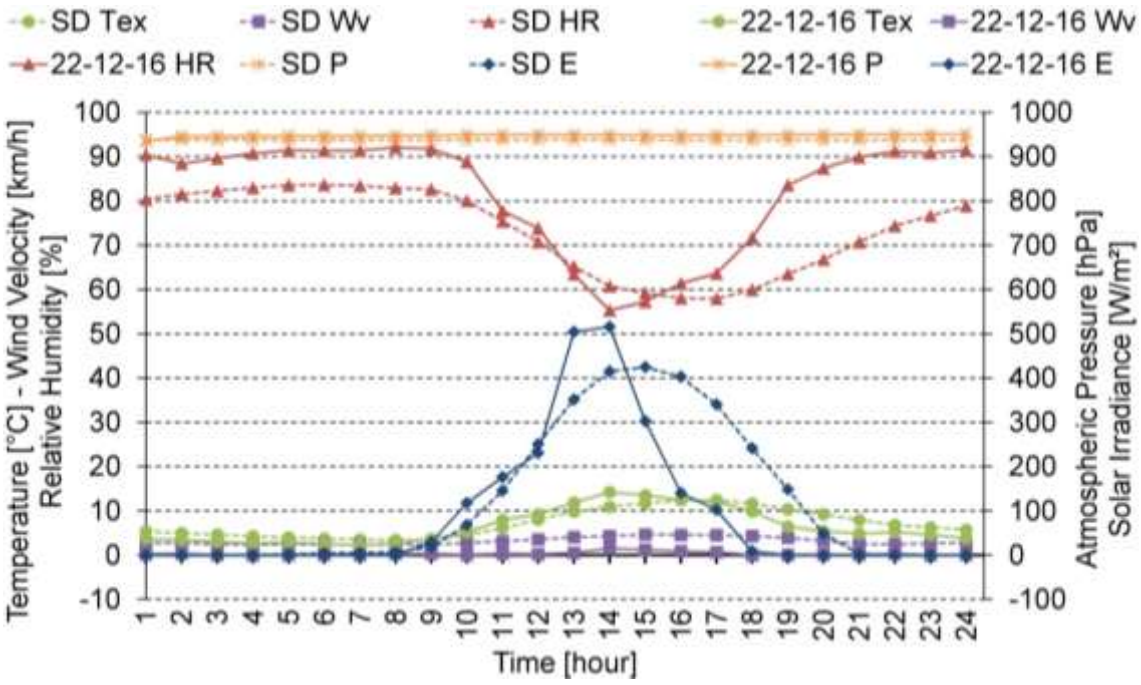

Figure 3. Comparison between the statistic day (SD) and case A (day 22-12-2016). Weather data include exterior temperature (Tex), wind velocity (Wv), relative humidity (HR), atmospheric pressure (P), and solar irradiance (E).

We calculated the local performance to evaluate the spatial effects of RG along the perimeter zone near a highly glazed façade (Section 2).

Local performance was represented by a plane with n = 81 points and defined by a grid span of 0.2 m with a variable distance (for the calculation of the view factor $F_{i,j}$ [47]) from the glass (i = 1,…9) and an opaque envelope (j = 1,…9).

The temperatures used for these charts were based on mean daily values for each day.

5. Experimental results and discussion

For the analysis, we compared three representative days: i) case A, as a typical day, 22-12-2016; ii) case B, as the coldest day, 31-12-2016; iii) case C, as the

warmest day, 30-01-2017. The weather data for these three days are illustrated in Table 6.

Case	Day	T_out ºC	Tmax ºC	Tmin ºC	HR %	P hPa	Wv km/h	Emax W/m²	Eday W·h/m²
A	22/12/2016	3.4	14.2	2.3	82	947.9	0.3	580.3	2128.0
B	31/12/2016	-0.5	2.9	-3.0	89	945.9	1.1	246.1	1124.1
C	30/01/2017	9.2	19.0	8.0	94	938.1	2.6	297.8	972.8

Table 6. Weather data for three days: mean daily exterior temperature T_out (ºC), relative humidity HR (%), atmospheric pressure P (hPa), maximum solar irradiance Emax (W/m²), total daily irradiance Eday (Wh/m²), and mean wind velocity Wv (km/h)

5.1 Glass characterization and surface temperatures

Interior and exterior mean surface temperatures of the glass (Figure 4 and Figure 5) are considerably different, with a gradient between the centre and the borders, depending on the edge effect (Figure 4, Figure 5).

In the reference cell (M5), the surface temperatures have the same fluctuation as T_out, because they depend directly on heat losses through the glass (Figure 4).

In the RG cell (M6), the surface temperatures do not exhibit the same fluctuation in T_out (Figure 5). In the interior, they depend directly on the RG; in the exterior, they mainly depend on the RG and negligibly on T_out.

The surface temperatures of the glass are observed to exhibit considerable fluctuations over a span of one hour, especially for the RG cell. This can be explained considering the following:

- in the reference cell (M5), there is a 1 °C tolerance for the temperature setting, due to the heating system (HVAC split unit).
- in the prototype cell (M6), the surface temperature of the RG was fixed as 30 ºC and the centre of the module was 21 ºC. Thus, when the RG reached 30 ºC it switched off and its temperature decreased rapidly (high thermal conductivity of the glass) until the thermostat in the centre of the cell (21 ºC with an accuracy of 1 ºC) switched the RG system on again. Although the thermostat positioned in the centre of M6 has an oscillation of 1 ºC, the RG could reach an oscillation of 7-9 ºC (Figure 5).

In addition, it is observed that in the middle of the day in cases A and C, the heating systems were not working, because the indoor temperatures were above 21 ºC and the glass surface temperatures were more stable; thus, no heating was required. This did not occur in case B, because of a low outdoor temperature.

The surface temperatures of the opaque envelope are similar in both cells.

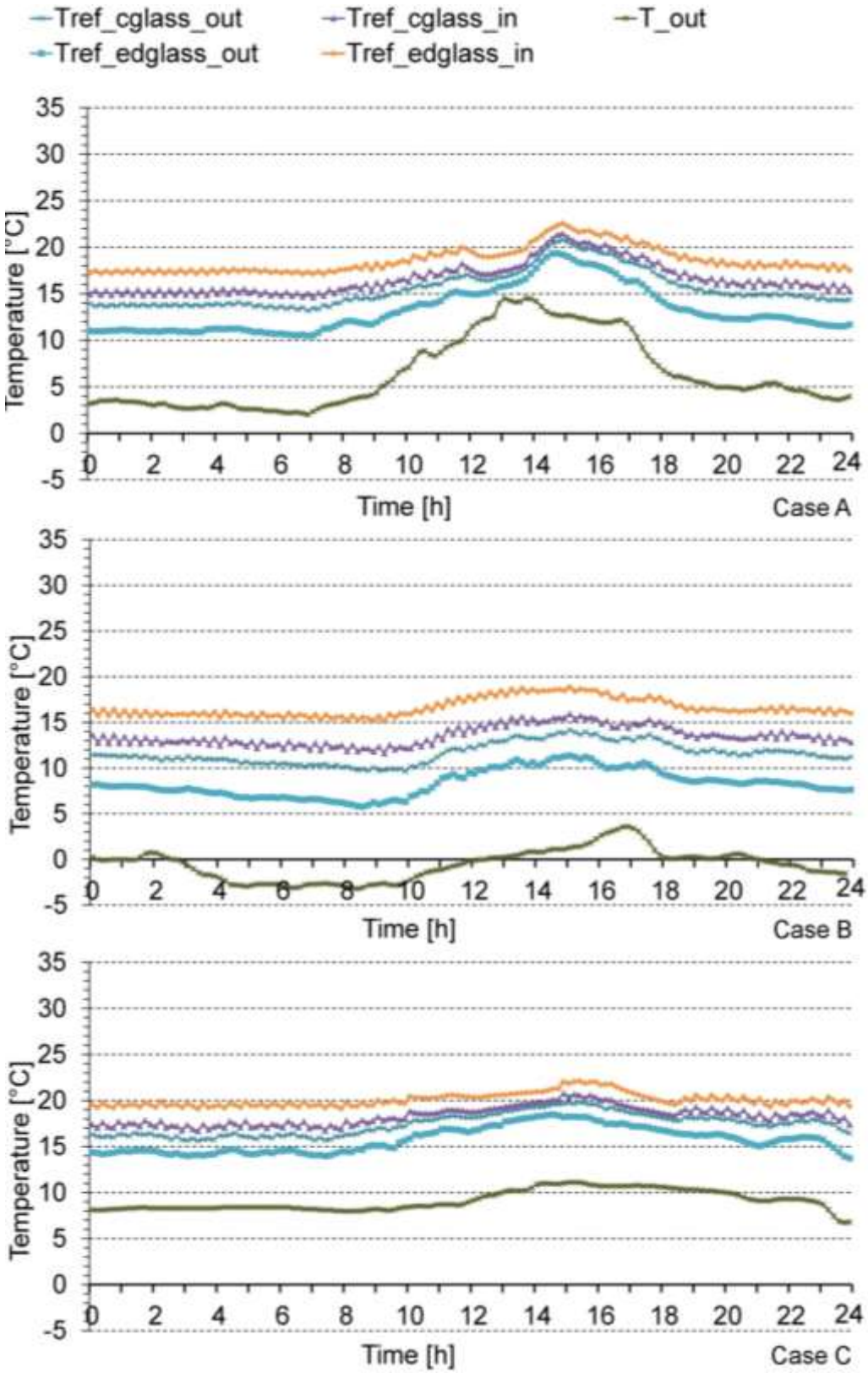

Figure 4. Comparison between exterior (Tref_cglass_out) and interior (Tref_cglass_in) centre pane temperatures, exterior (Tref_edglass_out) and

interior (Tref_edglass_in) border pane temperatures, and exterior temperatures (T_out) in the reference cell

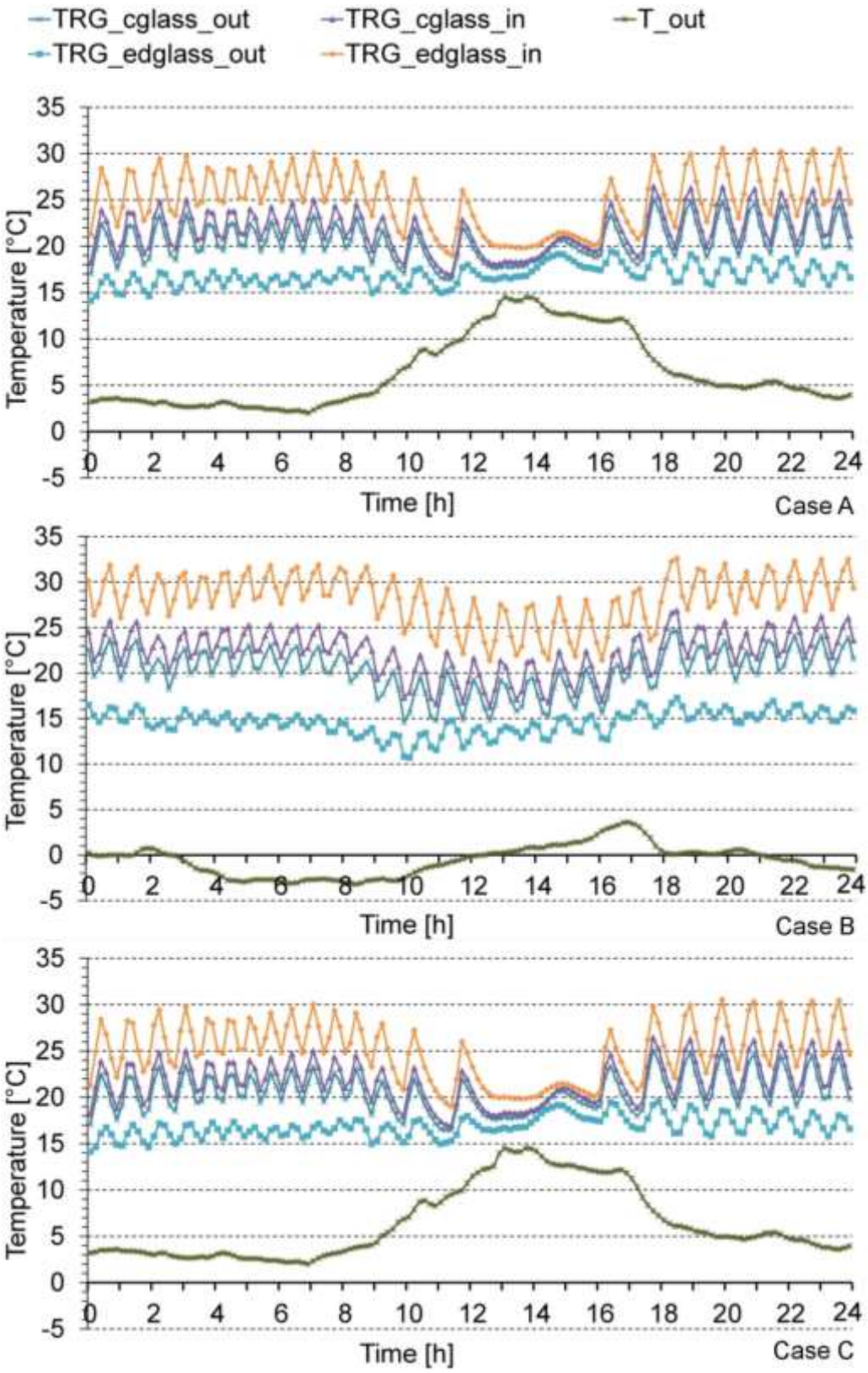

Figure 5. Comparison between exterior (TRG_cglass_out) and interior (TRG_cglass_in) centre pane temperatures, exterior (TRG_edglass_out) and

interior (TRG_edglass_in) border pane temperatures, and exterior temperatures (T_out) in RG cell

5.2 Operative temperature

In cases A and B, the air temperatures (T_air) in the reference and RG cells oscillate around 21 ºC, following the settled parameters; in case C they fluctuate between 21 ºC and 22 ºC (because of the warm day).

In reference cell (M5), the air temperature is higher than the glass temperature (with a difference of ≈ 2.8 ºC in case A, ≈ 4.8 ºC in case B, and ≈ 2.0 ºC in case C) and lower than the envelope temperature (with a difference of ≈ 2.3 ºC in case A, ≈ 2.7 ºC in case B, and ≈ 2.4 ºC in case C).

In the RG cell (M6), the air temperature is lower than the glass temperature (with a difference of ≈ 3.2 ºC in case A, ≈ 6.0 ºC in case B, and ≈ 2.1 ºC in case C) and lower than the envelope temperature (with a difference of ≈ 2.2 ºC in case A, ≈ 2.2 ºC in case B, and ≈ 1.8 ºC in case C).

In the reference cell, the daily averages of operative temperature (t_o) were 21.6 ºC in case A, 21.6 ºC in case B, and 22.4 ºC in case C. In all three cases, operative temperatures were higher than the air temperatures and followed the same fluctuation trend as exterior temperature (Figure 6).

In the RG cell, the daily averages of operative temperature (t_o) were 22.1 ºC in case A, 22.2 ºC in case B, and 22.0 ºC in case C. In all three cases, operative temperatures were higher than air temperatures (Figure 7) and independent of

the exterior temperature, due to the effect of the radiant temperature from the RG.

According to ISO 7730 [13] (table A5, annex A) the adequate value of t_o should be 22 ± 1 ºC.

Considering the data gathered from the RG cell (M6), t_o always satisfies the ISO requirements, even in case B (coldest day) when exterior temperature was approximately -3 ºC (at 9 a.m.). The slope of the t_o curve does not depend on exterior temperature.

In the reference cell (M5), almost all of the data meet the ISO [13] requirements (97.2% for case A and 90.3% for case B). However, most of the values are in the lower part of the permitted range of ±1 ºC (of 22ºC), indicating that the air temperature cannot be lowered to satisfy the requirements (20 ºC of minimum). It is also observed that the slope of the t_o curve depends on the exterior temperature, and only in case C (the warmest day) do the values reach the upper part of the range (94%).

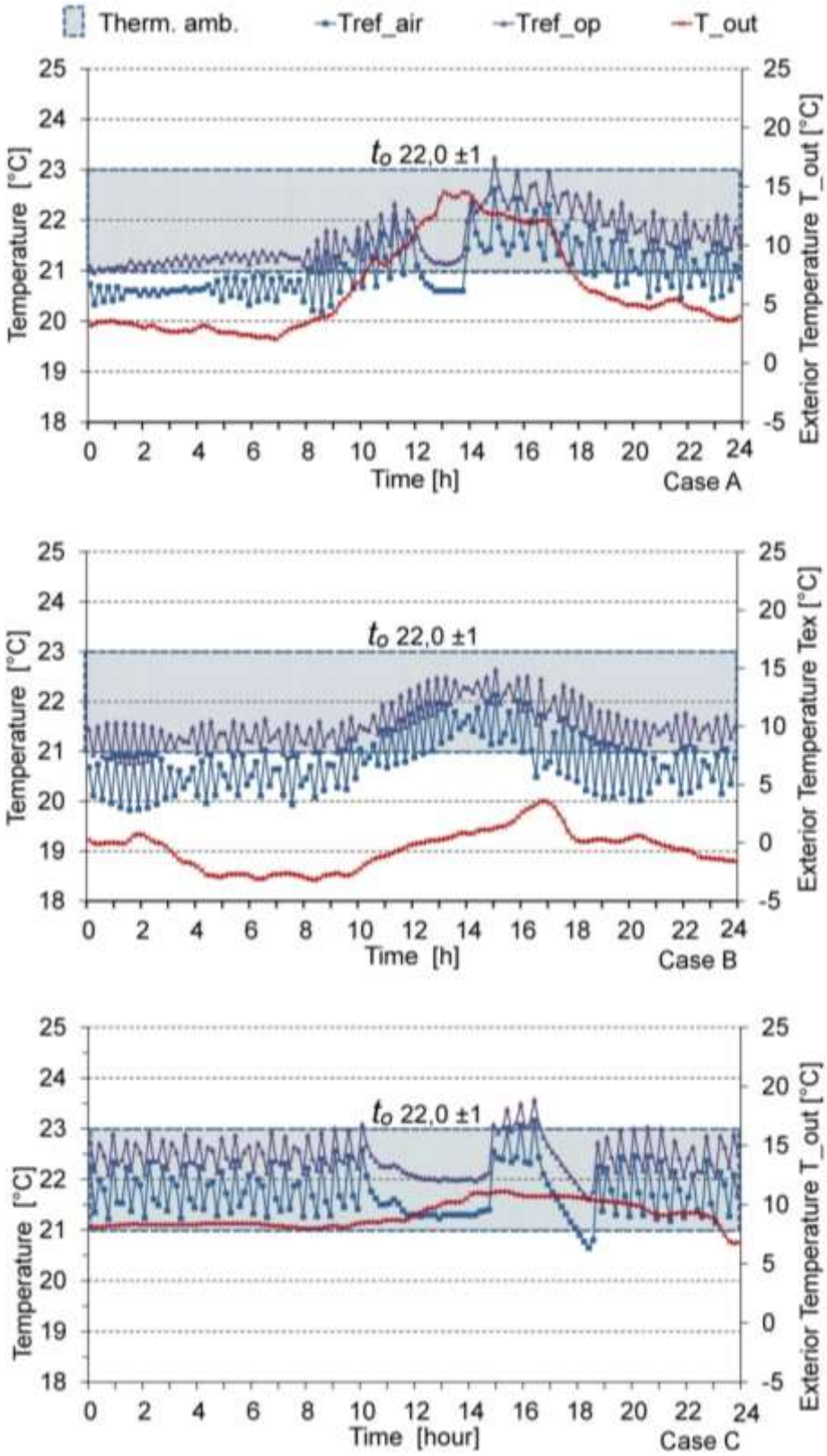

Figure 6. Comparison between operative (Tref_op), air (Tref_air), and exterior temperatures (T_out) in reference cell (ref, M5) for cases A, B, and C. The grey area represents thermal ambient category A (ISO 7730 [13] for office space).

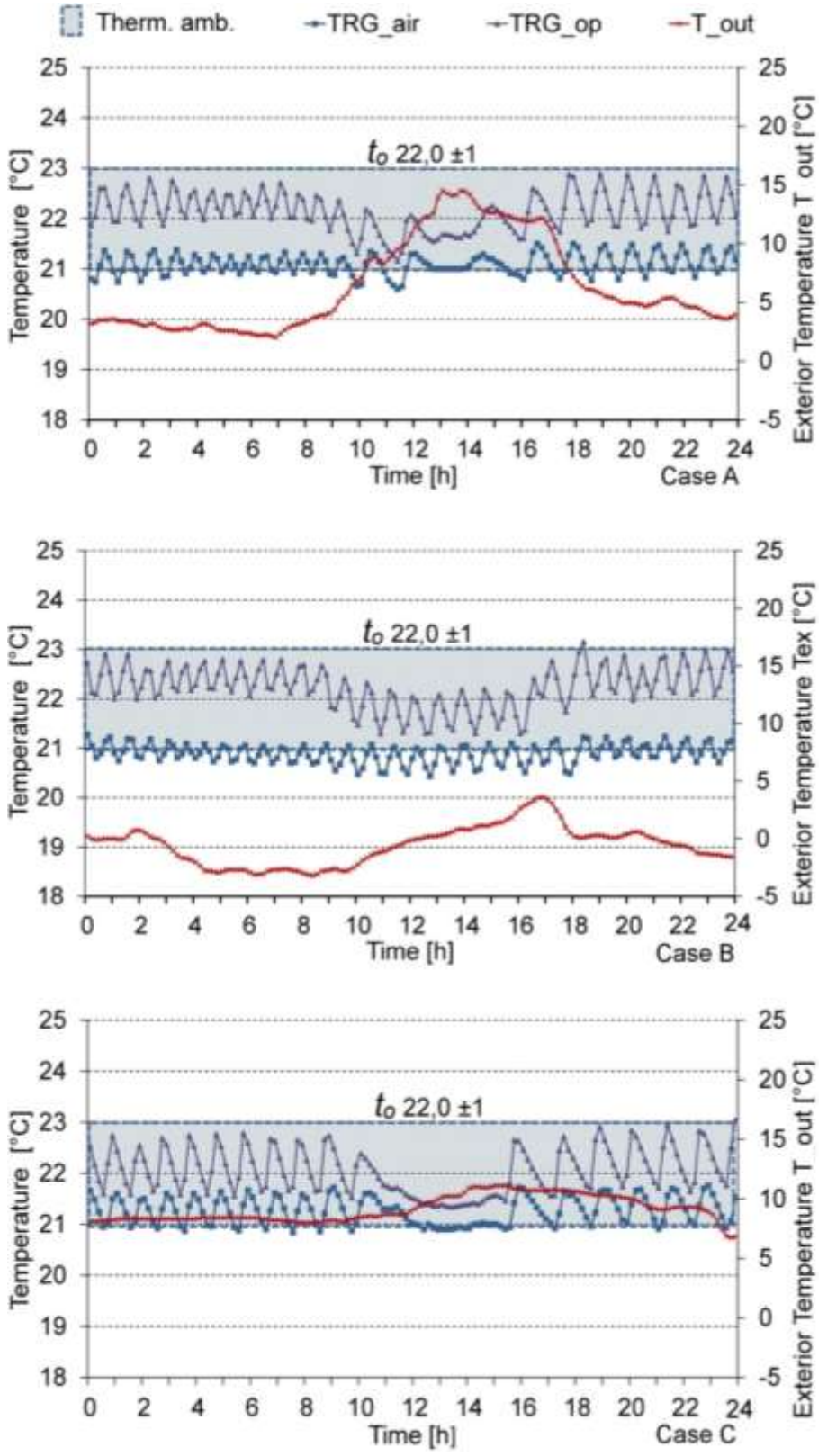

Figure 7. Comparison between operative (TRG_op), air (TRG_air), and exterior temperatures (T_out) in RG cell (RG, M6) for cases A, B, and C. The grey area represents thermal ambient category A (ISO 7730 [13] for office space).

5.3 Radiant temperatures and radiant asymmetry

The mean radiant temperatures ($\overline{t_r}$ in the centre of the cell) in the three cases (Figure 8):

- Case A: The daily average was 22.3 ºC in the reference cell (M5) and 23.2 ºC in the RG cell (M6), with a difference of 0.9 ºC.

  Considering the distribution during the day, the values of RG were usually higher than the values of the reference cell (80.6%).
- Case B: The daily average was 22.3 ºC in M5 and 23.6 ºC in M6, with a difference of 1.3 ºC.

  Considering the distribution during the day, the values of RG were usually higher than the values of the reference cell (86.6%).
- Case C: The daily average was 23.2 ºC in M5 and 22.8 ºC in M6, with a difference of 0.4 ºC.

  Considering the distribution during the day, the values of RG were 30.6% higher than the values of the reference cell.

In cases A and B (cold days) the RG maintained the inner glass surface temperature (in RG) between 22 ºC and 30 ºC, influencing $\overline{t_r}$ most of the time. In case C (warm day) the RG was on only part of the day because of the high exterior temperature. Therefore, the RG maintained a higher $\overline{t_r}$ in the RG cell than the $\overline{t_r}$ in the reference cell, but only during that part of the day.

Furthermore, considerable oscillations were observed in an interval of one hour, explained by the fluctuations of the glass, as described in Section 5.1.

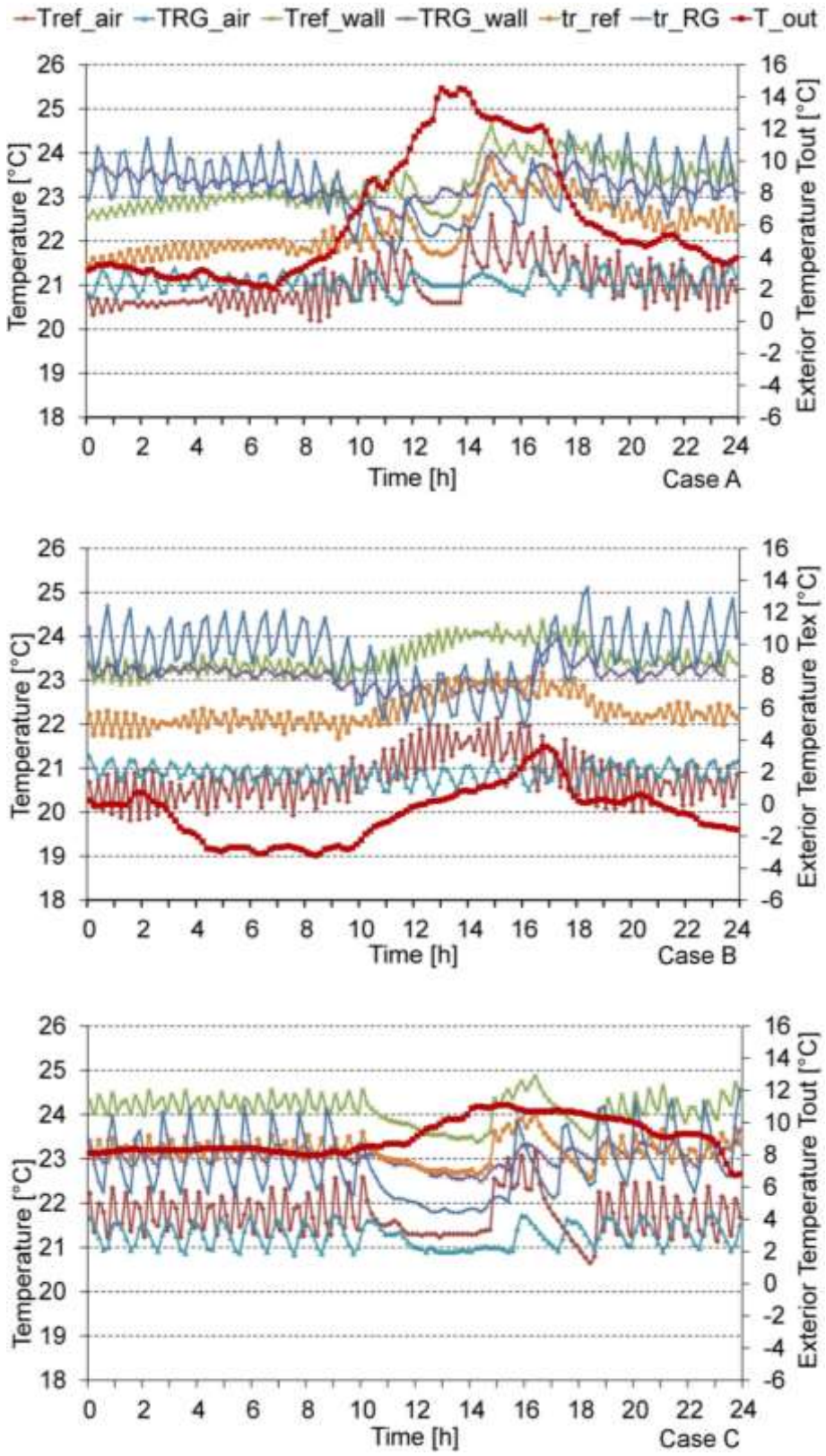

Figure 8. Comparison between mean radiant temperature (tr_ref, tr_RG), air temperature (Tref_air, TRG_air), interior wall temperature (Tref_wall, TRG_wall), and exterior temperature (T_out) in reference (ref) and RG cells.

The local distribution of the mean radiant temperature $\bar{t}_r$ in the reference cell was non-uniform. It was lower near the glass (≈ 21.5 ºC in case A, ≈ 21.1 ºC in case B, and ≈ 22.5 ºC in case C) with a gradient from the glass towards the back (Figure 9), and differences of 1.6 ºC in case A, 2.1 ºC in case B, and 1.4 ºC in case C.

The local distribution of $\bar{t}_r$ in the RG cell was almost uniform in cases A and C, with a minimum gradient (≈ 0.5 ºC and ≈ 0.3 ºC, respectively) towards the back (Figure 10). This is because $\bar{t}_r$ in the RG cell exhibited spatial uniformity. In case B, $\bar{t}_r$ was non-uniform with a longitudinal gradient of ≈ 1.4 ºC, because of the cold day with a higher difference between glass and envelope temperatures (Figure 10).

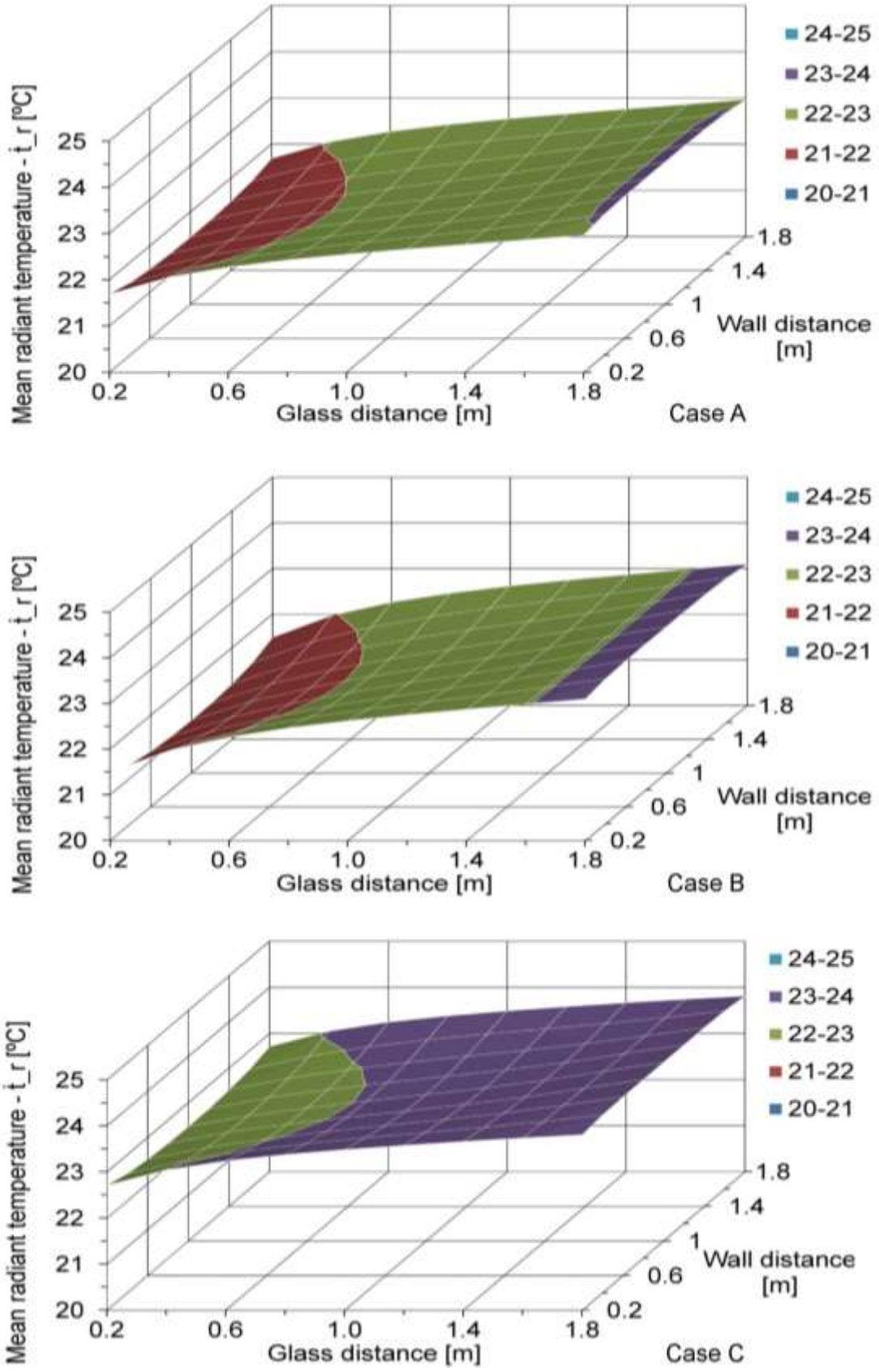

Figure 9. Local distribution of the mean radiant temperature ($\bar{t}_r$) in the reference cell

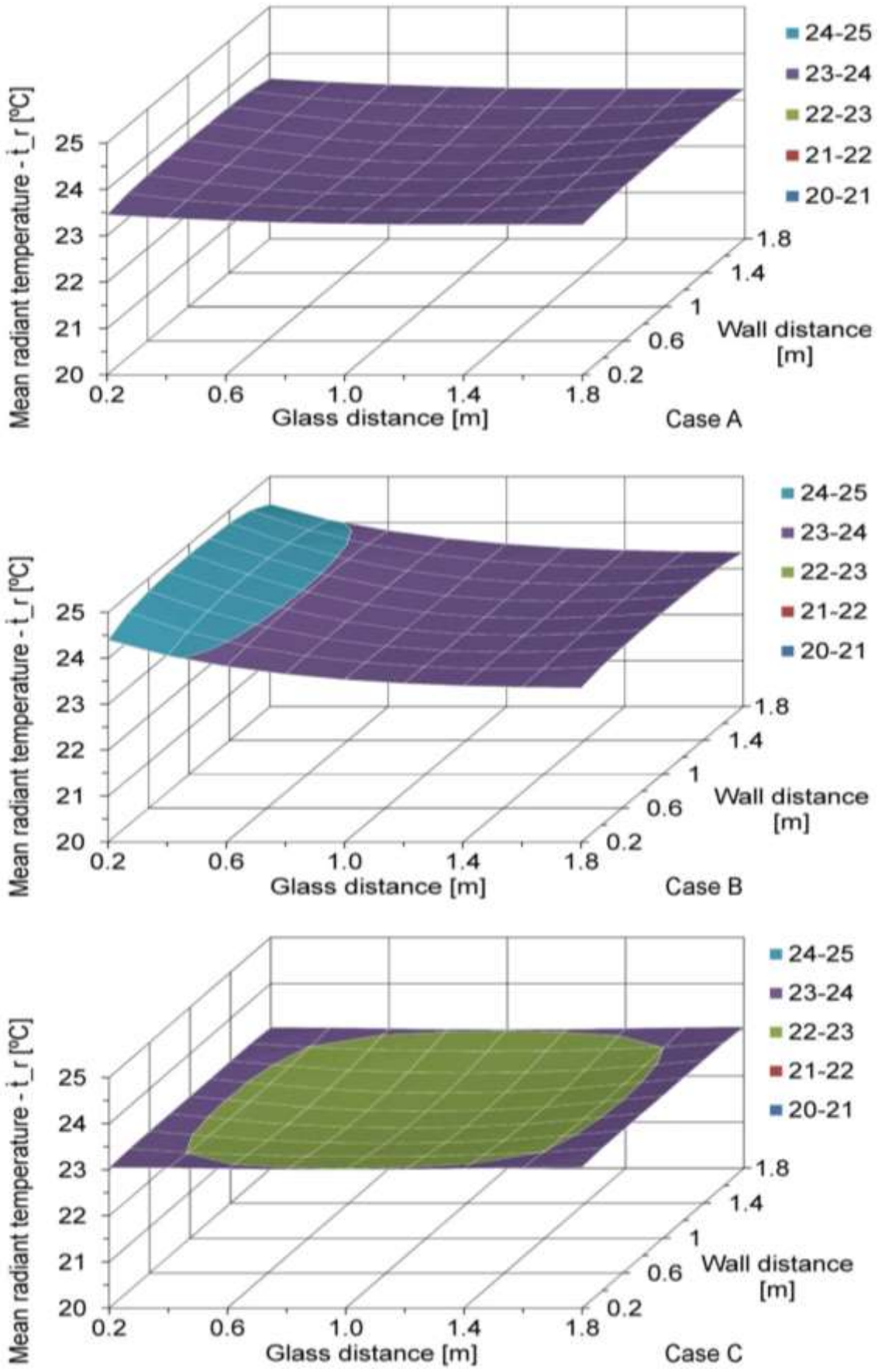

Figure 10. Local distribution of the mean radiant temperature ($\bar{t}_r$) in the RG cell

In the reference cell, the plane radiant temperature t_{pr} near the centre of the glass was 20.9 ºC in case A, 19.9 ºC in case B, and 21.9 ºC in case C.

In the RG cell, the t_{pr} near the centre of the glass was 23.7 ºC in case A, 25.1 ºC in case B, and 23.5 ºC in case C.

The differences between reference and RG cells were 2.78 ºC in case A, 5.2 ºC in case B, and 1.6 ºC in case C.

The difference in radiant temperature asymmetry Δt_{pr} between reference and RG cells at the centre glass (0.2 m from the glass) in all three cases was ≈ 4.2 ºC (Figure 11 and Figure 12).

Thus, the RG in all three cases has the same effect on Δt_{pr}, and does not depend on exterior conditions.

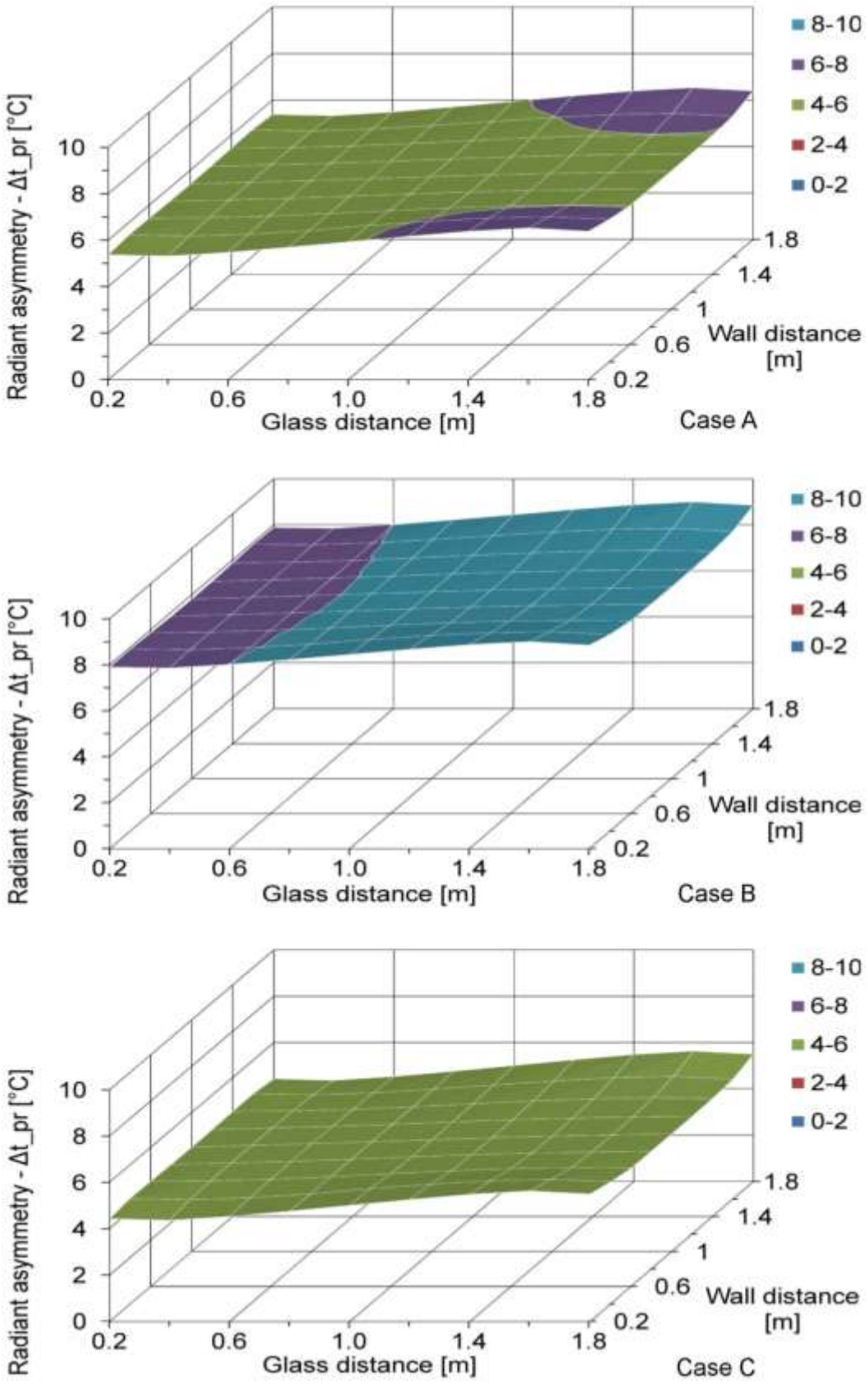

Figure 11. Local distribution of the radiant asymmetry temperature Δt_pr in the reference cell

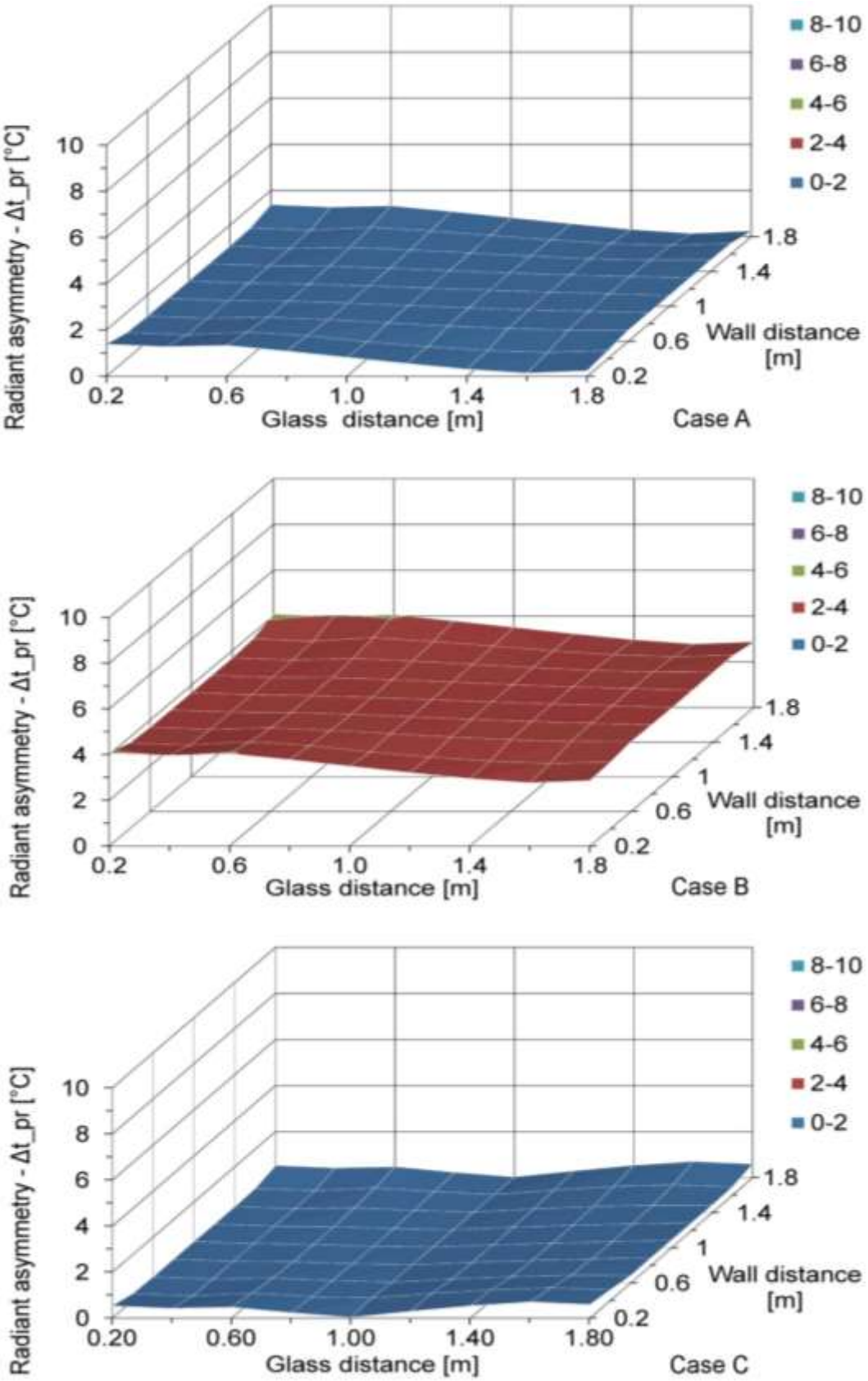

Figure 12. Local distribution of the radiant asymmetry temperatures Δt_pr in the RG cell

5.4 Thermal comfort performance

The thermal comfort analysis was based on the indices proposed by Fanger [5] and included in ISO 7730 [13].

The thermal environment categories were evaluated according to table A.1 of ISO 7730 and table A.1 of ISO 15251 [49], as presented in Table 7. The ISO 15251 do not consider criteria for local discomfort factors caused by radiant temperature asymmetry and PD index.

Thermal sensation scale	**Category**		**Thermal state of the body as a whole**		**Local discomfort radiant asymmetry**
ISO 7730/15251	**ISO 15251**	**ISO 7730**	**PPD %**	**PMV**	**PD %**
Neutral	I	A	<6	-0.20<PMV<+0.20	<5
Slightly warm/cool	II	B	<10	-0.50<PMV<+0.50	<5
Warm/Cool	III	C	<15	-0.70<PMV<+0.70	<10
Hot/Cold	IV	-	>15	PMV<-0.70 or PMV >+0.70	-

Table 7. Sensation scale and categories of thermal environment, according to ISO 7030 [13] and ISO 15251[49]

To estimate the thermal indoor quality of the cells, the methodology presented in the ISO and developed by Marino **Error! Reference source not found.** was used. Table 2 of the ISO [13], which defines the distribution of the individual thermal sensation votes for different values of the mean vote associated with the seven-point thermal sensation scale, was also considered.

Due to the considerable oscillations in the RG cell within a 10-minute span of data, a one-hour average was assessed for the analysis of parameters in both cells, which meets the hourly criteria indicated in ISO 15251 [49].

Time was divided into three periods (0:00 < P1 < 10:00, 10:00 < P2 < 16:00, and 16:00 < P3 < 24:00) according to the behaviours of the curves describing the interior comfort performance indices (Figure 13). The periods also coincide with the times when the RG was on (P1 and P3) and off (P2, due to the warm hours in the middle of the day).

The frequencies of the PMV indices were evaluated, and are within the range of values for the four categories of thermal environments (as described in Section 2) [49].

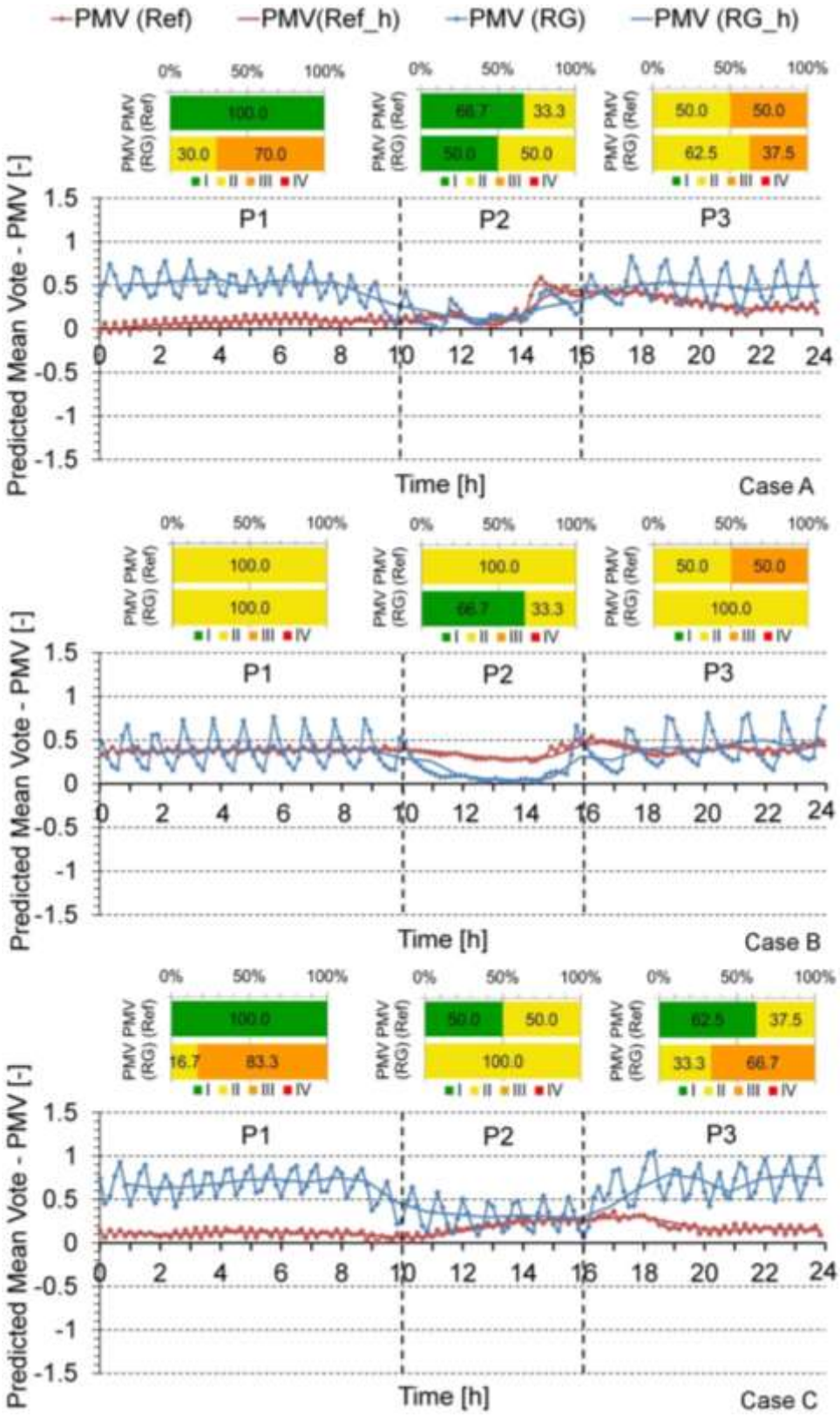

Figure 13. Comparison between the PMV index values [13] (10-minutes and 1-hour) and frequency included in the four thermal categories defined in ISO 15251 [49] (for periods P1, P2, and P3)

5.4.1 Comfort performance in reference cell (M5)

In the reference cell (M5), comfort performance during the three periods is summarized as follows (Figure 13):

- Period P1: In cases A and B, the values correspond to Category I, with a neutral sensation (considering the thermal sensation scale in Table 7). In case C, the values correspond to Category II, with a slightly warm thermal sensation. The higher category of case C results from the high exterior temperatures of the warm day.
- Period P2: In case A, the values mainly correspond to category I (66.7%), with a fraction in category II. In case B, the values correspond equally to category I and II. In case C, the values correspond to category II.

  The values are as expected in P2, as with P1.
- Period P3: In case A, the values correspond equally to category II and category III. In case B, the values correspond to category I (62.5%), with a fraction in category II. In case C, the values correspond equally to category II and category III.

The PPD has the same frequency as the PMV, according to its definition as a function derived from the PMV [13].

5.4.2 Comfort performance in RG cell (M6)

In the RG cell (M6), comfort performance during the three periods is summarized as follows (Figure 13):

- Period P1: In cases A and B, the values mainly correspond to category III (70% for A and 83.3% for B) with a warm sensation (considering the thermal sensation scale in Table 7), with a fraction in category II (30% for A and 16.7% for B). In case C, all values correspond to category II, with a slightly warm thermal sensation.

  This can be explained by higher PMV in cases A and B, influenced by RG that is usually on in P1. The PMV is lower in case C because of the warm day and reduced use of RG.
- Period P2: In case A, the values correspond equally to categories I and II. In case B, all values correspond to category III. In case C, the values mainly correspond to category III (66.7%). P2 is the warmest part of the day with less RG use, affecting the results of all three cases.
- Period P3: In case A, the values mainly correspond to category II (62.5%) (slightly warm thermal sensation), with a fraction in category III (37.5%). In case B, the values mainly correspond to category III (66.7%) (warm thermal sensation), with a fraction in category II (33.3%). In case C, all values correspond to category II (slightly warm thermal sensation).

  As with P1, in cases A and B, the PMV is higher due to RG that is usually on during the period. The PMV is lower in case C because of the warm day.

It is concluded that in the RG cell, the values of the thermal comfort indices are higher than in the reference cell for case A (typical winter day) and case B (coldest day). Cases A and B represent the warmest thermal environment categories; for adequate comfort indices: the mean radiant temperature can be decreased by decreasing the RG temperature, or can be maintained by decreasing the air temperature.

The PPD has the same frequency as the PMV in the same categories, according to its definition as a function derived from the PMV [13].

5.5 Local distribution of comfort performance

For the analysis of the local distribution of comfort performance, the definition in Section 4.4 and the daily mean values of the surface temperatures of the cells were used.

In the reference cell (M5), the local distribution of the PMV shows similar surface configurations in all three cases (Figure 14) with an accentuated increase from the façade to the bottom:

- In case A, the minimum value of -0.1% (class A, neutral thermal sensation) increases to a maximum of +0.4% (class B, slightly warm), with a difference of ≈ 0.5.
- In case B, the minimum value of -0.2% (class B, slightly cool thermal sensation) increases to a maximum of +0.4% (class B, slightly warm), with a difference of ≈ 0.7.
- In case C, the minimum of +0.1% (class A, neutral) increases to a maximum of +0.6% (class C, warm thermal sensation), with a difference of ≈ 0.5.

In all three cases, the curve describes a significant change in comfort from the glass to the back wall, explained by the cooling effect of the glass compared to the opaque walls ($\overline{t}_r$ glass < $\overline{t}_r$ walls); the PMV is higher with cold outside temperatures.

In the RG cell (M6), the local distribution of the PMV differed between cases:

- Cases A and C show a similar configuration (Figure 15), flat from the façade to the bottom wall, with values of ≈ +0.4% for case A and ≈ +0.5% for case C (class B indices with slightly warm thermal sensation).
- In case B, the distribution decreases from the façade to the bottom wall, from a maximum of +1.0% to a minimum of +0.6% (both values within class C, warm thermal sensation), with a difference of ≈ 0.4.

In cases A and C, the curves are almost flat, because they depend on the RG to produce a warming effect ($\bar{t}_r$ glass ≈ $\bar{t}_r$ walls), similar to the opaque walls. These behaviours are different from those of a typical glass façade and are expected only for RG.

In case B, the curve increases from the glass to the back wall because of the warming effect of the RG that is usually on as a result of the cold day (Figure 10).

It is concluded that in the reference cell, the degree of comfort changes with a considerable gradient from the glazed façade to the opaque bottom envelope. These behaviours are as expected for a typical glass façade.

In the RG cell, for cases A and C, the degree of comfort is constant; for case B, the RG system produces a warming effect that is greater than desired, even on the coldest day. This suggests that to have a neutral thermal sensation in an RG cell, the mean radiant temperature should be reduced, which could be accomplished without any reduction in comfort level along the perimeter zone near the façade. Reducing the surface temperature of the RG or reducing the air temperature to maintain the mean radiant temperature may have the same effect.

In the reference cell, this reduction is not possible, due to local discomfort near the glass produced by the non-uniform distribution of thermal conditions.

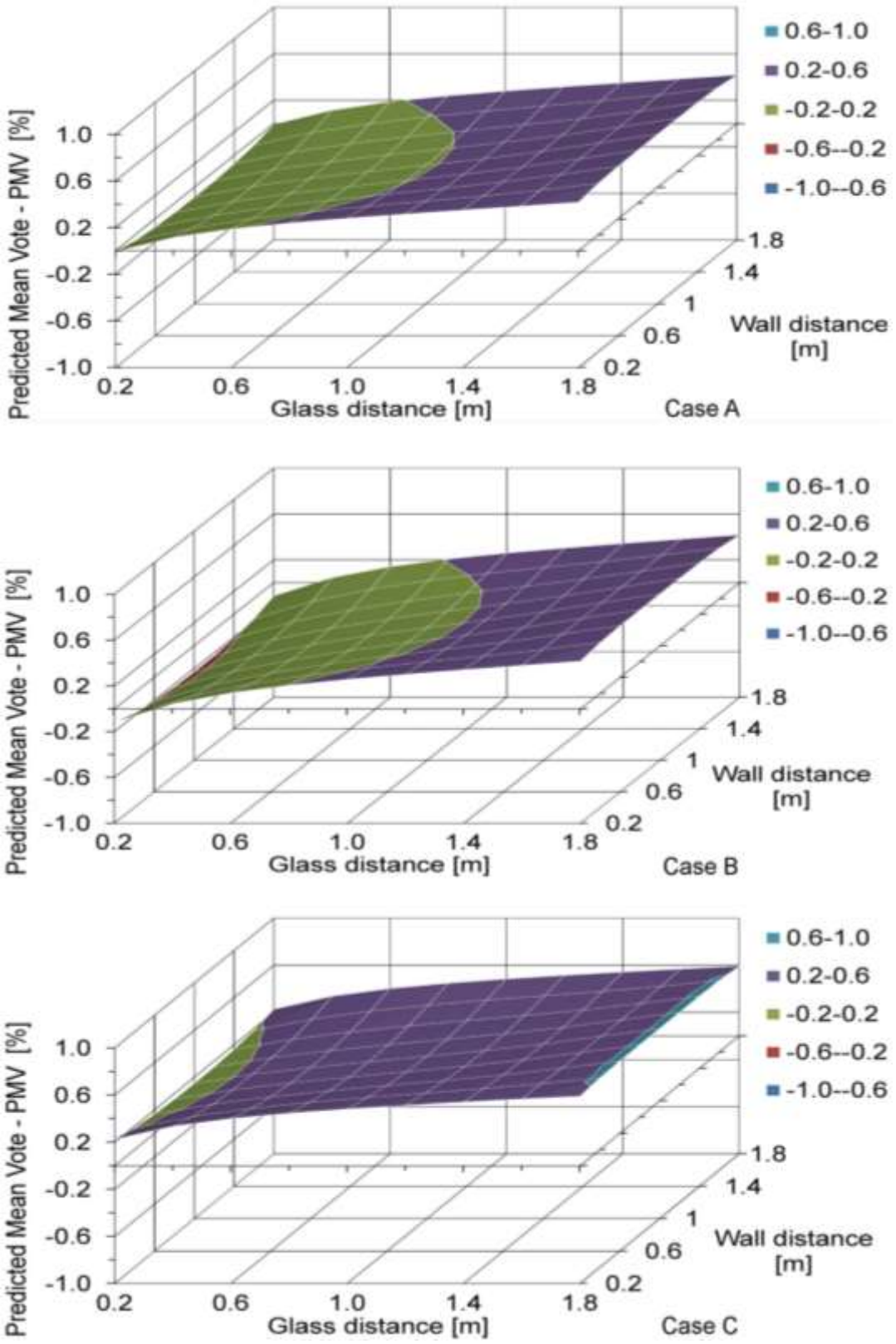

Figure 14. Local distribution of the PMV in the reference cell (M5)

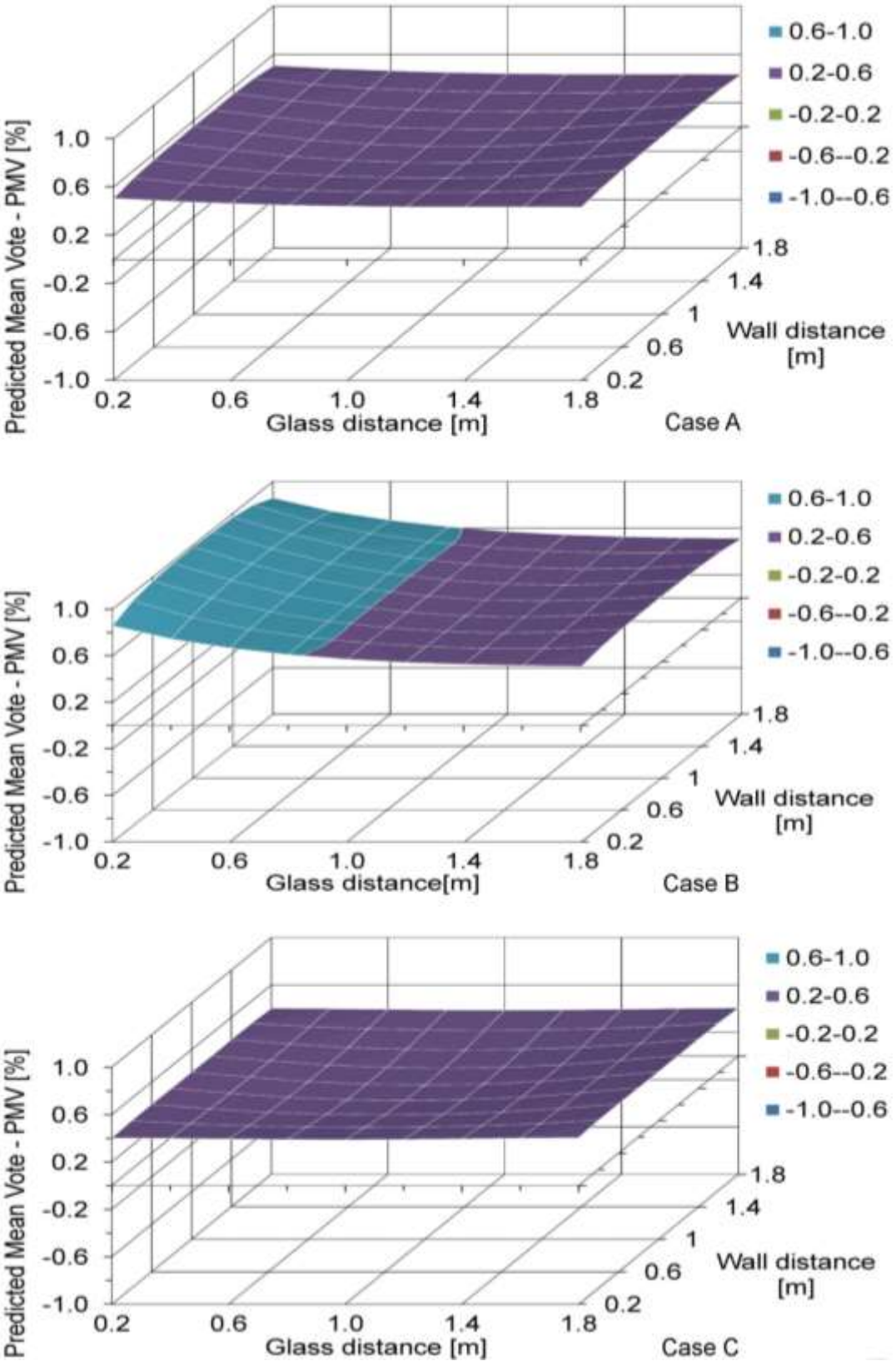

Figure 15. Local distribution of the PMV in the RG cell (M6)

6. Conclusions

The objective of this study was to investigate the thermal and comfort performances of radiant glass technology compared to a conventional glass façade.

A comparative methodology was used to evaluate the results of the experiments conducted using outdoor twin cells.

Radiant glass (RG) technology was used to heat the prototype cell, and an HVAC device was used to heat the reference cell.

It was verified that the air temperatures in both cells were similar, and the mean radiant temperature and operative temperatures in the prototype cell (with RG) were higher than in the reference cell.

In the RG cell, variation during the day does not depend on the fluctuation of exterior conditions; in contrast, the reference cell with standard glass is affected by exterior conditions.

It has been demonstrated that RG technology can achieve a uniform distribution of $\bar{t}_r$ and t_{pr}, even along the perimeter zone near the façade, and is not dependent on the distance from the glass or exterior temperature. The difference between the two cells was greater in colder external conditions.

The radiant temperature asymmetry was lower in the RG cell and higher in the reference cell; the difference was ≈ 4.2 ºC (similar in all three cases).

In the RG cell, the indoor quality of the environment, evaluated according to the thermal environment categories recommended by international standards, was uniformly spatially distributed, even along the perimeter zone near the façade, and independent of exterior climatic conditions, unlike the reference cell with standard glass.

It was verified that the value of t_o in the RG cell, if settled according to the recommendation of the standards, produces a $\bar{t}_r$ that causes discomfort through warm thermal sensation. This suggests that to meet the recommended thermal comfort levels, it is necessary to reduce the operative temperature by reducing the mean radiant temperature, the RG surface temperature, or the air temperature. In the RG cell, this can be accomplished without any reduction in general or local comfort level along the perimeter zone, to maintain a low Δt_{pr}, even in cold weather conditions.

In the reference cell, such a reduction is not possible (the distributions of all indices are not spatially uniform) without producing a reduction in comfort levels throughout the perimeter zone.

Further investigation is required to define the degree of this reduction, compare the energy consumption, and evaluate the sustainability of RG technology.

This research did not receive any specific grant from funding agencies in the public, commercial, or not-for-profit sectors.

Acknowledgments

This paper is part of the ongoing PhD research project titled “Thermal behaviour of the radiant glass in the glazed envelope. Characterization and experimental simulation”. Also the authors are grateful to: Controlglass SL for the manufacture and supply of the glasses; Schüco Iberia SL to provide the façade frames; Department of Construction and Architectural Technology, School of Architecture, Polytechnic University of Madrid for the use of the Global Energy and Sustainable Laboratory facility.

REFERENCES

[1] T. Chown, C. Li, Z. Lin, Innovative solar windows for cooling-demand climate, Solar Energy Materials & Solar Cells, 94 (2) (2010) 212–220.

[2] E. Cuce, S.B. Riffat, A state-of-the art review on innovative glazing technologies, Renewable and Sustainable Energy Reviews 41 (2015) 695-714.

[3] B. Jelle, A. Hynd, A. Gustavsen, D. Arasteh, H. Goudey, R. Hart, Fenestration of today and tomorrow: A state-of-the-art review and future research opportunities, Solar Energy Materials & Solar Cells 96 (2012) 1-28.

[4] R. C. G. M. Loonen, J. M. Rico Martinez, F. Favoino, M. Brzezicki, C. Menezo, G. La Ferla, L. L. Aelenei, Design for façade adaptability: Towards a unified and systematic characterization, in: 10th Conference on Advanced Building Skins, Bern, Switzerland, 2015, 1284-1294.

[5] P.O. Fanger, Calculation of Thermal Comfort: Introduction of a basic comfort equation. ASHRAE Transactions 73 (2) (1967) III.4.1-III.4.20.

[6] C. Huizenga, H. Zhang, P. Mattelaer, T. Yu, E. Arens, P. Lyons, Window Performance for Human Thermal Comfort. Final Report to the National Fenestration Rating Council, Center for the Built Environment. University of California, Berkeley (2006).

[7] P.O. Fanger, L. Bànhidi, B.W. Olesen, G. Langkilde, Comfort limits for heated ceilings. ASHRAE Trans. 86 (2) (1980) 141-156.

[8] P.O. Fanger, B.M. Ipsen, G. Langkilde, B.W. Olessen, N.K. Christensen, S. Tanabe, Comfort limits for asymmetric thermal radiation, Energy and Buildings 8 (3) (1985) 225-236.

[9] D.A. McIntyre, Sensitivity and discomfort associated with overhead thermal radiation, Ergonomics 20 (3) (1977) 287-296.

[10] I.S. Griffith, D.A. McIntyre, Subjective response to overhead thermal radiation, Human Factors 16 (4) (1974) 415-422.

[11] Jr.P.E. Mcnall, R.E Biddison, Thermal and comfort sensations of sedentary persons exposed to asymmetric radiant fields. ASHRAE Transactions, 76 (1) (1970) 123-136.

[12] ASHRAE Standard 55-2004, Thermal environmental conditions for human occupancy, ASHRAE, Atlanta (2004).

[13] ISO 7730-2005, Ergonomics of the thermal environment — Analytical determination and interpretation of thermal comfort using calculation of the PMV and PPD indices and local thermal comfort criteria. International Standard Organization, Geneva (2005).

[14] B.W. Olesen, Thermal comfort requirements for floors, Proc. of the meeting of commissions B1, B2, E1 of IIR, Belgrade, (1977) pp. 337-343.

[15] B.W. Olesen, K.C. Parsons, Introduction to thermal comfort standards and to the proposed new version of EN ISO 7730, Energy and Buildings 34 (6) (2002) 537-548.

[16] F.R. d'Ambrosio Alfano, M. Dell'Isola, B.I. Palella, G. Riccio, A. Russi, On the measurement of the mean radiant temperature and its influence on the indoor thermal environment assessment, Build. Environ. 63 (2013.) 79-88.

[17] I. Atmaca, O. Kaynakli, A. Yigit, Effects of radiant temperature on thermal comfort, Build. Environ. 42 (2007) 3210-3220.

[18] M.C. Singh, S.N. Garg, R. Jha, Different glazing systems and their impact on human thermal comfort-Indian scenario, Build. Environ. 43 (2008) 1596-1602.

[19] M. Bessoudo, A. Tzempelikos, A.K. Athienitis, R. Zmeureanu, Indoor thermal environmental conditions near glazed facades with shading devices – Part I: experiments and building thermal model, Build. Environ. 45 (11) (2010) 2506-2516.

[20] M. R., Safizadeh, M., Schweiker, A., Wagner, Experimental Evaluation of Radiant Heating Ceiling Systems Based on Thermal Comfort Criteria, Energies 11 (2018) 1-21.

[21] H. Zhang, C. Huizenga, E. Arens, D. Wang, Thermal sensation and comfort in transient non-uniform thermal environments, Eur. J. Appl. Physiol. 92 (2004) 728-733.

[22] C. Huizenga, H. Zhang, E. Arens, D. Wang, Skin and core temperature responses in uniform and non-uniform, steady-state and transient thermal environments, Journal of Thermal Biology 29 (2004) 549-558.

[23] C. Marino, A. Nucara, M. Pietrafesa, Thermal comfort in indoor environment: Effect of the solar radiation on the radiant temperature asymmetry, Solar Energy 144 (2017) 295-309.

[24] M. Dawe, P. Raftery, J. Woolley, S. Schiavon, F. Bauman, Comparison of mean radiant and air temperatures in mechanically-conditioned commercial buildings from over 200,000 field and laboratory measurements, Energy and Buildings 206 (2020) 109582.

[25] J. Babiak, B.W. Olesen, D. Petras, Low Temperature Heating and High Temperature Cooling. REHVA Guidebook No 7, 1st ed., Federation of European Heating and Air conditioning Associations, Belgium (2009).

[26] S. Oxizidis, A.M. Papadopoulos, Performance of radiant cooling surfaces with respect to energy consumption and thermal comfort. Energy and Build. 57 (2013) 199-209.

[27] M. Gwerder, B. Lehmann, J. Tödtli, V. Dorer, F. Renggli, Control of thermally activated building systems (TABS), Appl. Energy 85 (2008) 565-581.

[28] M. Gwerder, J. Tödtli, B. Lehmann, V. Dorer, W. Güntensperger, F. Renggli, Control of thermally activated building systems (TABS) in intermittent operation with pulse width modulation, Appl. Energy 86 (2009) 1606-1616.

[29] H., Jia, X., Pang, P., Haves, Experimentally-determined characteristics of radiant systems for office buildings, Appl. Energy 221 (2018) 41-54.

[30] C. Karmann, S. Schiavon, F. Bauman, Thermal comfort in buildings using radiant vs. all-air systems: A critical literature review. Building and Environment 111 (2017) 123-131.

[31] C., Karmann, S., Schiavon, L.T., Graham, P., Raftery, F., Bauman, Comparing temperature and acoustic satisfaction in 60 radiant and all-air buildings. Building and Environment 126 (2017) 431-441.

[32] G. Gan, Analysis of mean radiant temperature and thermal comfort, Build. Serv. Eng. Res. Technol. 22 (2001) 95-101.

[33] U. Larsson, B. Moshfegh, Experimental investigation of downdraught from well-insulated windows, Building and Environment 37 (2002) 1073-1082.

[34] ASHRAE, ASHRAE Handbook, Fundamentals SI edition, American Society of Heating, Refrigerating and Air-Conditioning Engineers, Atlanta (2010).

[35] Real Decreto 1751/1998 de 31 de julio (BOE. 5 de agosto de 1998), por el que se aprueba el Reglamento de Instalaciones Térmicas en los Edificios (RITE) y sus Instrucciones Técnicas Complementarias (ITE). Versión consolidada, Septiembre 2013 [In Spanish].

[36] A. Tzempelikos, M. Bessoudo, A.K. Athienitis, R. Zmeureanu, Indoor thermal environmental conditions near glazed facades with shading devices – Part II: Thermal comfort simulation and impact of glazing and shading properties, Building and Environment 45 (11) (2010) 2517-2525.

[37] J. Le Dréau, P. Heiselberg, Sensitivity analysis of the thermal performance of radiant and convective terminals for cooling buildings. Energy and Buildings 82 (2014) 482-491.

[38] R. S. Tender, P. F. Gerhardinger, A. Millet, Insulating glass with capacitively coupled heating system, US 5.852.284, Perrysburg, Ohio, 22th of December, 1998.

[39] A. Moreau, S. Sansregret, F. Fournier, Modelling and Study of the Impacts of Electrically Heated Windows on the Energy Needs of Buildings, in: 6th IASME / WSEAS International Conference on Heat Transfer, Thermal, Engineering and Environment (IHTE'08), Rhodes, Greece, 2008.

[40] J. Kurnitski, J. Jokisalo, J. Palonen, K. Jokiranta, O. Seppänen, Efficiency of electrically heated windows, Energy and Buildings 36 (2004) 1003-1010.

[41] A. E. Ollokiegi, Electric heated windows: Thermal comfort and energy use aspects. Master Thesis in Energy Systems, Gävle: University of Gävle, 2013.

[42] H. S. Jammulamadaka, Evaluation of Energy Efficiency Performance of Heated Windows, Graduate Thesis, Dissertations, and Problem Reports. 5879, 2017.

[43] G. Cattarin, F. Causone, A. Kindinis, L. Pagliano, Outdoor test cells for building envelope experimental characterisation – A literature review. Renewable and Sustainable Energy Reviews 54 (2016) 606–625.

[44] V. Serra, F. Zanghirella, M. Perino, Experimental evaluation of a climate façade: Energy efficiency and thermal comfort performance, Energy and Buildings 42 (1) (2010) 50–62.

[45] Berkeley Lab WINDOW 7.4.14 and Optics 6.0 software, Lawrence Berkeley National Laboratory, this version contains Glass Library records from IGDB (Spectral Data) Version 29.0

[46] ISO, ISO 13731-2001, Ergonomics of the thermal environment - Vocabulary and symbols, International Standard Organization, Geneva, 2001.

[47] ISO, ISO 7726-2001, Ergonomics of the thermal environment. Instruments for measuring physical quantities, International Standard Organization, Geneva, 2001.

[48] G. Cannistraro, G. Franzitta, C. Giaconia, G. Rizzo, Algorithms for the calculation of the view factors between human body and rectangular surfaces in parallelepiped environments, Energy and Buildings 19 (1) (1992) 51–60.

[49] CEN, ISO 15251-2007. Indoor environmental input parameters for design and assessment of energy performance of buildings – addressing indoor air quality, thermal environment, lighting and acoustics. European Standardisation Organisation, Brussels, 2007.

[50] C. G. Granqvist, A. Hultaker, Transparent and conducting ITO films: new developments and Applications, Thin Solid Films, 411 (1) (2002) 1–5.

[51] P. Gerhardinger, Next generation heated glass products, Appliance (60) 28-32, https://business.highbeam.com/5622/article-1G1-106097092/nextgeneration-heated-glass-products-heated-glass-has, 2003 [Accessed: 20/12/2012].

[52] G. La Ferla, C. Acha, J. Roset, El vidrio calentado eléctricamente y su eficiencia energética como sistema de calefacción en una envolvente acristalada, In: Primer Congreso Internacional Sobre Investigación en Construcción y Tecnología Arquitectónicas, Madrid: Esquela Técnica Superior de Arquitectura, Madrid, 2014 [In Spanish].

[53] G. La Ferla, GESLAB. Global Energy and Sustainable Laboratory in Building Relative test-cells fully exposed to outdoor, in: Building Performance Simulation and Characterisation of Adaptive Facades – Adaptive Facade Network, F. Favoino, R.C.G.M. Loonen, M. Doya, F. Goia, C. Bedon, F. Babich (Eds.), TU Delft Open for the COST Action 1403 adaptive facade network, 2018, pp. 145.

[54] O. Kalyanova, P. Heiselberg, Experimental Set-up and Full-scale measurements in “The Cube”, Aalborg: Department of civil engineering, Aalborg University, DCE Technical reports, No. 34, 2008.

[55] A. Chazarra, A. Barcelo Mestre, V. Pires, M. Mendes, J. Neto, Iberian Climate Atlas. Air temperature and precipitation (1971-2000). Agencia Estatal de Meteorología, Ministerio de Medio Ambiente y Medio Rural y Marino, Instituto de Meteorología de Portugal, Closas-Orcoyen, 2011.

[56] M. Kottek, J. Grieser, C. Beck, B. Rudolf, F. Rubel, World Map of the Köppen-Geiger climate classification updated, Meteorologische Zeitschrift 15 (3) (2006) 259-263.

[57] AEMET, Valores climatológicos normales. Madrid, Cuatro Vientos, http://www.aemet.es/es/serviciosclimaticos/datosclimatologicos/valoresclimatologicos?l=3196&k=mad, 2017, [Accessed: 16/10/2017].

[58] M. Luo, X. Zhou, X. Zhu, J. Sundell, Revisiting an overlooked parameter in thermal comfort studies, the metabolic rate, Energy and Buildings 118 (2016) 152–159.

[59] ISO, ISO 15099-2003. Thermal performance of windows, doors and shading devices — Detailed calculations. Revised in 2016. International Standard Organization, Geneva, 2016.

[60] C. Marino, P. Misiani, A. Nucara, M. Pietrafesa, The effect of the climatic condition on the radiant asymmetry, Int. J. Heat Technol. 35 (1) (2017) 419-426.

[61] C. Marino, A. Nucara, M. Pietrafesa, Proposal of comfort classification indexes suitable for both single environments and whole buildings. Building and Environment 57 (2012) 58-67.